haematologica
Journal of The Ferrata Storti Foundation

# Intravenous iron preparations transiently generate non-transferrin-bound iron from two proposed pathways

by Maciej W. Garbowski, Sukhvinder Bansal, John B. Porter, Claudio Mori, Susanna Burckhardt, and Robert C. Hider

Haematologica 2020 [Epub ahead of print]

*Citation: Maciej W. Garbowski, Sukhvinder Bansal, John B. Porter, Claudio Mori, Susanna Burckhardt, and Robert C. Hider. Intravenous iron preparations transiently generate non-transferrin-bound iron from two proposed pathways.*
*Haematologica. 2020; 105:xxx*
*doi:10.3324/haematol.2020.250803*

# Title Page

The title:
**Intravenous iron preparations transiently generate non-transferrin-bound iron from two proposed pathways**

Names of authors:
Maciej W. Garbowski,[1-3] Sukhvinder Bansal,[2] John B. Porter,[1] Claudio Mori,[4] Susanna Burckhardt,[4] Robert C. Hider[2,3]

Authors' Affiliations:
[1]University College London (UCL) Cancer Institute Haematology Department; [2]King's College London (KCL) Institute of Pharmaceutical Science; [3]London Metallomics Consortium, UK; [4]Vifor Pharma Group, Glattbrugg, Switzerland

Running heads: NTBI following intravenous iron administration

Contact information for correspondence:
Maciej Garbowski, Haematology Department, University College London Cancer Institute, Paul O'Gorman Building, 3rd Floor, 72 Huntley Street, WC1E 6BT London, UK. E-mail: maciej.garbowski@ucl.ac.uk; phone: +44 207 679 6233, fax: +44 207 679 6224

Word count:
Text approx. 4,321
Abstract 250
Number of Tables 2
Number of Figures 6
Number of references 62

## Abstract

Intravenous iron-carbohydrate complex preparations (IVIPs) are non-interchangeable pro-drugs: their pharmacokinetics (PK) varies determined by semi-crystalline iron core and carbohydrate shell structures, influences pharmacodynamics (PD) and thus efficacy and safety. Examining PK/PD relationships of 3 IVIPs we identify a two-pathway model of transient NTBI generation following single dose administration.

28 hypoferremic non-anemic patients randomized to 200mg iron as ferric carboxymaltose (Fe-carboxymaltose), iron sucrose (Fe-sucrose), iron isomaltoside 1000 (Fe-isomaltoside-1000), n=8/arm, or placebo, n=4, on a 2-week PK/PD study, had samples analysed for total serum iron, IVIP-iron, transferrin-bound iron (TBI) by HPLC-ICP-MS, transferrin saturation (TSAT), serum ferritin (s-Ferritin) by standard methods, non-TBI (NTBI) and hepcidin as published before. IVIP-dependent increases in these parameters returned to baseline in 48-150h, except for s-Ferritin and TSAT. NTBI was low with Fe-isomaltoside-1000 (0.13µM at 8h), rapidly increased with Fe-sucrose (0.8µM at 2h, 1.25µM at 4h), and delayed for Fe-carboxymaltose (0.57µM at 24h). NTBI AUCs were 7-fold greater for Fe-carboxymaltose and Fe-sucrose than for Fe-isomaltoside-1000. Hepcidin peak time varied, but not AUC or mean levels. s-Ferritin levels and AUC were highest for Fe-carboxymaltose and greater than placebo for all IVIPs. We propose 2 mechanisms for the observed NTBI kinetics: rapid and delayed NTBI appearance consistent with direct (circulating IVIP-to-plasma) and indirect (IVIP-to-macrophage-to-plasma) iron release based on IVIP plasma half-life and s-Ferritin dynamics.

IVIPs generate different, broadly stability- and PK-dependent, NTBI and s-Ferritin signatures, which may influence iron bioavailability, efficacy and safety. Longer-term studies should link NTBI exposure to subsequent safety and efficacy parameters and potential clinical consequences.

## Introduction

NTBI collectively refers to a heterogeneous group of plasma iron species that are not bound to transferrin, ferritin or heme typically present with TSAT>75%[1,2]. In iron overload conditions these are thought to comprise ferric citrate species, mostly albumin-bound, some of which are more redox-active than others[3]. NTBI species, present in iron-overloaded patients, are responsible for the pattern of atypical tissue iron distribution seen under such conditions, including extrahepatic (endocrine and myocardial) haemosiderosis[4]. However, the IVIP itself is not considered to represent NTBI, or the redox-active, weakly-bound species, although it can become the source of both. Following IVIP infusion, in principle, NTBI could be generated by either a rapid iron egress from macrophages following primary uptake into the macrophage system or by intravascular iron release from the circulating IVIP prior to macrophage uptake. The structure of the IVIP being administered is likely to influence the levels and duration of both NTBI components. These are largely un-described however, and are compared here for three different IVIPs.

IVIPs have become increasingly used in the treatment of iron deficiency within the context of a wide range of diseases[5]. All of these preparations are pro-drugs[6,7] for bioavailable iron but their exact mode of iron delivery is unclear[5]. This remains poorly recognised despite their widespread use[5]. It has been suggested that, depending on the nature of the carbohydrate shell, some IVIPs partly decompose in plasma before macrophage uptake; their subsequent endolysosomal degradation releases iron for transient storage or export to plasma[8].

Available IVIPs include iron sucrose (Fe-sucrose), ferric carboxymaltose (Fe-carboxymaltose), sodium ferric gluconate, iron isomaltoside 1000 (Fe-isomaltoside-1000), ferumoxytol, and low molecular weight iron dextran. Depending on the carbohydrate shell type, these preparations can be classified as non-dextran-based and dextran/dextran-based complexes[9]. Non-dextran-based complexes exhibit a correlation between molecular weight (MW) distribution and complex stability, i.e. higher MW complexes are more stable and have lower labile iron content than lower MW complexes. In contrast, dextran/dextran-based complexes are all very stable independent of their MW [5,10].

Here, we selected two non-dextran-based IVIPs with different MW distributions, Fe-carboxymaltose (Ferinject®, 145–155kDa) and Fe-sucrose (Venofer®, 42–44kDa), as well as a dextran-based complex Fe-isomaltoside-1000 (Monofer®, 63–69kDa)[5]. The purpose of this study was to examine the NTBI profiles in the context of other PK/PD parameters under identical conditions (200mg iron dose administered over 10 min), in hypoferremic, otherwise healthy, subjects, to better understand their mode of action. Previous studies showed that all three preparations are known to transiently increase TSAT with decay half-lives $t_{1/2}$=23h (Fe-isomaltoside-1000), $t_{1/2}$=8h (Fe-carboxymaltose), and $t_{1/2}$=5h (Fe-sucrose)[11], possibly with associated NTBI[12,13]. Crucially however, appropriate NTBI and TSAT methods are necessary that distinguish between IVIP-Fe, TBI and NTBI. We used a highly sensitive and specific bead-based NTBI assay that is robust to transferrin[1,14]. This means that due to the hexadentate nature of the assay chelator on the beads (CP851) iron is neither removed from ferrotransferrin nor donated (shuttled) to apotransferrin, thus minimizing nonspecific overestimation or underestimation of NTBI, respectively[1,14].

Different IVIPs display different iron pharmacokinetics, dependent on the structure of the semi-crystalline iron core and the type of polysaccharide ligand[7,15]. Such properties may influence IVIP efficacy and safety[11,16], but also inform the mechanisms of iron delivery and IVIP differences. Pharmacokinetics, stability, and the amount of weakly-bound iron, define the maximal single dose that can be administered[5]. This is relevant, as the increased IVIP use is also linked to the fact that, with new preparations, high doses can be given in a short amount of time. Therefore, following a single dose of 200mg iron, we monitored, among others, the pharmacokinetics of the IVIPs, TSI (TBI, NTBI and IVIP-Fe), TSAT, hepcidin and s-Ferritin levels over a period of 2 weeks. Although there have been some direct comparisons between different IVIPs[17–19], none have compared the above six parameters in man, over a two-week period. This approach has allowed us to identify two proposed pathways of NTBI generation in IVIP treatment.

## Methods

### Study design and patient population

Our work is part of an exploratory Phase 1 single-centre, single-blind, randomised, placebo-controlled study to describe and characterise the PK and PD of Fe-carboxymaltose, Fe-sucrose, and Fe-isomaltoside-1000 in hypoferremic non-anemic subjects. 28 subjects (Hb ≥13g/dl for males, and ≥12g/dl for females, fasting s-Ferritin<30µg/l and TSAT<20% measured at 08:00-09:00 a.m.) randomised into 1 of 3 treatment groups (n=8/arm), or 1 placebo control group (n=4/arm), received a single intravenous 200 mg iron dose of Fe-carboxymaltose, Fe-sucrose or Fe-isomaltoside-1000, or saline solution (placebo) over 10 minutes. Blood samples, processed for serum and batch-frozen at -80ºC, were taken on Day -1 at 08:00-09:00, then 4 and 12h later (baseline iron profile); on Day 1 immediately pre-dose at 08:00-09:00 (time: 0 minutes), 10 (immediately post-dose), 20, and 40 minutes, then 1, 2, 4, 6, 8, 12, 16, 24h, then 36, 48, 72, 96, 120, 144, and 312-336h post-dose. The study was approved by a local Ethics Committee and all patients gave informed consent on entering the study.

### Serum iron profiles and s-Ferritin levels

Vifor Pharma performed all assays except as stated.
TSI was measured using a validated inductively Coupled Plasma Optical Emission Spectroscopy method. Unsaturated iron binding capacity (UIBC) was measured by a photometric colorimetric test (Beckman Coulter UIBC Metabolite assay). TBI was calculated as *TBI[µmol/l]=(transferrin[g/l]x25.12)-UIBC[µmol/l]* where transferrin concentration was measured immuno-turbidimetrically (Beckman Coulter Transferin assay). Conversion of TBI units:
*TBI[µg/ml]=TBI[µmol/l]x55.845[µg/µmol]x0.001[l/ml].* TSAT was calculated as *TSAT[%]=100–(3.98×UIBC[µmol/l]/transferrin[g/l]).* UIBC values below the lower limit of quantification were imputed as 0 in the TBI formula. S-Ferritin was measured with a Chemiluminescent Microparticle Immunoassay (Architect systems), hemoglobin and reticulocytes using standard methods, and soluble transferrin receptor-1 (sTfR1) by particle-enhanced immunonephelometry (N Latex sTfR assay). IVIP-Fe was determined subtracting TBI from TSI[20].

### Non-transferrin-bound iron

We used the previously published bead-NTBI method[1,14] with some modifications (Supplement). Serum samples or buffered solutions incubated with the CP851 beads were assayed by flow-cytometry (Beckman Coulter CytoFLEX, CytExpert software, KCL) and quantitated against ferric nitrilotriacetate (Fe-NTA) standards (Figure 1). Limit of Blank was 0.51nM, Limit of Detection 14.6nM, Limit of Quantitation 30nM; intra-assay and inter-assay precision CVs were 1.28% and 4.34%, respectively (further details in Supplement).

### Plasma Hepcidin

Plasma hepcidin (KCL) was measured in serum samples using tandem mass spectrometry[21]; for detailed method, see Supplement.

### Inductively-Coupled Plasma Mass-Spectrometry serum analyses

A parallel set of serum samples (baseline, 4-312h) was also analyzed by HPLC-ICPMS at KCL to measure IVIP-Fe and examine the chromatographic behavior of IVIPs. Perkin Elmer Flexar HPLC coupled to a Perkin Elmer NexION 350 D Inductively-Coupled Plasma Mass Spectrometer was used with Syngistix and Chromera operating software (Figure 2A). Sample preparation, instrumentation, and measurement of IVIP iron in plasma, are detailed in the Supplement.

### Statistical Analysis

All data is presented as mean±SD, unless otherwise stated. Analysis of Variance (ANOVA) with a post-test Holm-Sidak's multiple comparisons test was used to compare means between treatments. Pharmacokinetics parameters were derived from non-compartmental analysis for all subjects using Full Analysis Set ($c_{max}$, half-life, and $t_{max}$ are shown). Area-under-curve (AUC) and nonlinear regression analysis using global fitting was performed on GraphPad Prism (version 6.0). A p value<0.05 was considered statistically significant.

## Results

### Chromatographic behaviour of IVIPs in serum

In order to examine the chromatographic behaviour of the IVIPs in serum, buffered solutions of Fe-carboxymaltose, Fe-sucrose, Fe-isomaltoside-1000 (30µM) were mixed with normal human serum (80/20 vol/vol) and the mixtures were incubated in vitro for 1h on the bench top. Samples spiked with the internal standard ferrioxamine (FO) were then injected into HPLC-ICPMS. IVIP chromatograms in 20% serum are shown as subtraction plots, with control chromatograms subtracted (Figure 2B, 2C, 2D). Ferrotransferrin peak appears at 13.17min as a result of rapid iron exchange with apotransferrin (stoichiometric amount of apotransferrin was subtracted) either during the short sample processing at the bench and/or waiting time in the auto-sampler, or directly on the column. The post-subtraction IVIP-Fe recovery was 28µM for Fe-carboxymaltose, 32µM for Fe-isomaltoside-1000, and 23.5µM for Fe-sucrose. Low recovery for Fe-sucrose appears likely due to multiple serial dilutions in ammonium acetate buffer (pH=7.4) to obtain 30µM, with some precipitation or re-speciation (Fe-sucrose pH 10.5-11.1). The subtraction chromatograms show that Fe-isomaltoside-1000 particularly is distributed very widely (peak at 11min, 126kDa), while Fe-carboxymaltose and Fe-sucrose have comparable species distribution peaking at

9.2min (160kDa) and 8.9min (165kDa), respectively. Notably, these elution times and therefore MW ranges do not correspond to the values obtained in the presence of buffers alone[5]. This difference results most likely from the in vivo formation of the protein corona[22] and probably aggregation between IVIP cores and plasma proteins.

### Patient baseline characteristics

Patients were balanced between arms for all the baseline parameters (Table 1) with the exception of gender. Screening s-Ferritin ranged between 2.85-27.54µg/L (percentiles 25$^{th}$, 50$^{th}$, 75$^{th}$: 8.49, 11.05, 17.78µg/L), TSAT: 5.11-19.62% (9.48, 14.00, 17.24%), and haemoglobin: 12.0-15.4 g/dL (12.5, 13.0, 13.4g/dL).

### Comparison of IVIP-Fe between treatments

There were striking differences in biomarker time-courses between IVIPs, as shown in Figure 3A-C. For the IVIP-Fe (as TSI-TBI), the elimination rate was slowest; while $c_{max}$ was highest with Fe-isomaltoside-1000, followed by Fe-carboxymaltose and Fe-sucrose (at median $t_{max}$ 0.67, 0.34, 0.35h, respectively), see Table 2. The $c_{max}$ was comparable within 95% CI for all IVIPs (spanning 1mM value): 1.29±0.1mM for Fe-isomaltoside-1000, 1.16±0.09mM for Fe-carboxymaltose, and 0.85±0.17mM for Fe-sucrose, Figure 4A, Table 2. The IVIP-Fe AUC differed between treatments ($p<0.0001$), with Fe-isomaltoside-1000 14-fold higher than Fe-sucrose and 3-fold higher than Fe-carboxymaltose, Fe-carboxymaltose 4.8-fold higher than Fe-sucrose ($p<0.0001$ for all pairs). The between-patient average IVIP-Fe half-life was 10-fold longer for Fe-isomaltoside-1000 (20.3±2.27h) and twice longer for Fe-carboxymaltose (6.82±1.93h) than for Fe-sucrose (3.43±1.55h), Table 2. The chromatographic behaviour of IVIPs was also monitored using HPLC-ICPMS at KCL (see Methods). Subtraction chromatograms (4h-baseline) show clear differences in IVIP-Fe profiles (Figure 2B), each presenting a distinct chromatographic behaviour: Fe-isomaltoside-1000 has a broad peak eluting at 11.3min, Fe-carboxymaltose at 9.36min and Fe-sucrose at 8.97min with a single principal peak each. These ex-vivo 100% serum profiles compare well with the in-vitro 20% serum profiles, Figure 2C (discussed).

### TSI changes between treatments

The time-courses of TSI closely follow the kinetics of IVIP-Fe, especially for Fe-isomaltoside-1000. For Fe-carboxymaltose and Fe-sucrose there is an early separation of IVIP-Fe from the trajectory of TSI (Figure 3A-C, green and red profiles, also compare Figure 4A and Figure B). This is a consequence of their half-life being much shorter, and thus IVIP-Fe decaying to sufficiently low values for the TBI component to dominate TSI. TSI $c_{max}$ is comparable, within 95% CI, across treatments, and TSI $t_{max}$ closely corresponds to IVIP-Fe $t_{max}$, Figure 4B, Table 2. The TSI AUC differed ($p=0.0001$) between treatments, with Fe-isomaltoside-1000 9.6-fold higher than Fe-sucrose and 2.6-fold higher than Fe-carboxymaltose, while Fe-carboxymaltose 3.7-fold higher than Fe-sucrose ($p<0.0001$ for all pairs).

### TSAT and NTBI changes between treatments

TSAT was lower with Fe-isomaltoside-1000 reaching 81.04±16.52% at 24h (range 60.5-100%) vs. early full saturation with Fe-sucrose (already at 2h 95.24±8.87%, range 79.2-100%), and later full saturation with Fe-carboxymaltose at 16h (97.00±8.49, range 76-100%), Figure 4C. TSAT AUC barely differed between treatments; for Fe-carboxymaltose vs. Fe-isomaltoside-1000 by only 32% ($p=0.048$) with other comparisons statistically insignificant.

NTBI was relatively low with Fe-isomaltoside-1000 (peak 0.13±0.27µM at 8h), but appeared high notably rapidly with Fe-sucrose (0.79µM±0.72µM at 2h, peak 1.25±0.61µM at 4h), and was delayed with Fe-carboxymaltose (peak at 0.58±0.43µM at 24h), Figure 4D. The first appearance of NTBI associated with relatively low TSAT, likely related to the rate of iron release from the IVIP. The peak NTBI values were associated with full TSAT (or near-saturation in Fe-isomaltoside-1000 group) and the disappearance of NTBI precedes (occurs before) the normalisation of TSAT, compare Figure 4C and Figure 4D. In contrast to TSAT AUC, the NTBI AUC differed significantly (p=0.01) between groups on average, with Fe-carboxymaltose nearly 7-fold higher than Fe-isomaltoside-1000 (p=0.04), Fe-sucrose vs. Fe-isomaltoside-1000 nearly 9-fold higher (p=0.01) while for Fe-sucrose vs. Fe-carboxymaltose only 1.15-fold higher (p=ns).

### Hepcidin changes between treatments

Hepcidin peaks earlier with Fe-sucrose to 68.6±34.7ng/mL at 24h, than with Fe-isomaltoside-1000 to 54.3±15.2ng/mL at 36h and than with Fe-carboxymaltose to 58.9±25.2ng/mL at 48h. All hepcidin AUCs were similar (p-value= 0.54), Figure 4E. This is in keeping with similar exposure of hepatocytes to TSAT (transferrin-$Fe_2$) between treatments: see above. Furthermore, it indicates the NTBI exposure (AUC) differences do not influence the exposure to hepcidin.

### S-Ferritin changes between treatments

S-Ferritin showed significant differences between treatments, increasing faster with time for both Fe-sucrose and Fe-carboxymaltose and slower for Fe-isomaltoside-1000. Ferritin increase from ~12µg/L at baseline was greatest for Fe-carboxymaltose to ~200µg/L at 72h with an exponential constant k=0.028±0.013µg/L*h, followed by Fe-sucrose to ~150µg/L at 36h k=0.076±0.022µg/L*h, and Fe-isomaltoside-1000 to ~102µg/L at 96h, k=0.021±0.014µg/L*h (Figure 4F, Figure 5A,C). Ferritin AUC differed between groups (p<0.0001), Fe-carboxymaltose being 75% higher (p=0.007) than Fe-isomaltoside-1000 and 63% higher (p=0.01) than Fe-sucrose, with comparable AUCs for Fe-isomaltoside-1000 and Fe-sucrose (p=0.98). All IVIPs had greater ferritin AUC vs. placebo: 9-, 10-, and 16-fold for Fe-isomaltoside-1000, Fe-sucrose and Fe-carboxymaltose, respectively, Figure 5B.

S-Ferritin iron content changes between treatments and the erythropoietic response are presented in the Supplement.

## Discussion

NTBI typically appears as the primary pathological culprit of parenchymal haemosiderosis[23] in chronic iron overload conditions: hereditary hemochromatosis[24], thalassemias[25], sickle cell anemia[26], rare anemias[27,28], myelodysplasia[29,30] and myoloablation[31,32]. Different NTBI species and other factors[33] may determine variable distribution of tissue haemosiderosis[4]. NTBI levels vary by disease, degree of transfusion dependence, and the assays used to detect them[2,34], but can be as high as 8.5µM[35]. In contrast, NTBI appearance is transient after oral or IV iron administration. In studies of single dose oral iron at doses equivalent to 100 mg of ferrous sulphate, NTBI concentrations measured by various methodologies ranged 1-6 µM[36–39]. In this study, maximal NTBI concentrations ranged from 0.13 to 1.25 µM

(Fe-sucrose>Fe-carboxymaltose>Fe-isomaltoside-1000), being at the lower end of concentrations observed after oral administration. We also measured labile plasma iron[40] which reflects the activity of redox-active NTBI subspecies, but its levels were lower than measured NTBI concentrations (0.83, 0.15 and 0.18 µM for Fe-sucrose, Fe-isomaltoside-1000 and Fe-carboxymaltose, respectively, data not shown). NTBI appearance associated with oral or IV iron administration has been associated with acute increases in non-specific biomarkers of oxidative stress in clinical studies[41–44]. However, several epidemiologic studies and a recent prospective clinical trial have not shown that IVIP administration is associated with adverse cardiovascular outcomes[45,46]. Analyses of large dialysis patient datasets have shown modest associations with increased infections at higher doses, however, this was not observed in the recent prospective clinical trial in chronic kidney disease patients[47,48].
Although NTBI appearance following oral[36–39,49] and intravenous iron administration of different formulations is described[17,18,50], here we present a unique study directly comparing 3 IVIPs (Fe-isomaltoside-1000, Fe-sucrose, Fe-carboxymaltose). We compared 6 associated iron metabolism parameters over 2 weeks with complex kinetics unique to each formulation identified for the first time.
We reported increases in IVIP-Fe, TSI, TSAT, s-Ferritin, hepcidin, and NTBI, which returned to baseline within 2 weeks or sooner, except for s-Ferritin and TSAT (Figure 3-5). Based on the corresponding AUCs, Fe-isomaltoside-1000 resulted in the highest TSI exposure but the lowest TSAT, s-Ferritin, and NTBI. Fe-sucrose resulted in the lowest TSI exposure, intermediate TSAT and s-Ferritin exposure but highest NTBI exposure. Fe-carboxymaltose resulted in intermediate TSI and NTBI exposure, but highest TSAT and s-Ferritin exposure. Increased hepcidin levels were similar for the 3 IVIPs. Thus, the exposure to bioavailable iron, as judged from s-Ferritin and TSAT AUC, was highest for Fe-carboxymaltose, followed jointly by Fe-sucrose and Fe-isomaltoside-1000. For the latter two preparations, kinetics of iron bioavailability differed in that the short-term bioavailability rate was markedly greater for Fe-sucrose due to its known more limited stability profile (Figure 5A green vs. black curve)[6].
Although head-to-head comparison studies between Fe-carboxymaltose, Fe-sucrose, and Fe-isomaltoside-1000 looking at clinically meaningful outcomes are lacking, we speculate that relatively higher iron bioavailability for Fe-carboxymaltose could be responsible for the positive effect shown on outcomes in heart failure in comparison with oral iron[51–53].
This is the first report of IVIP-Fe kinetics measured directly for Fe-isomaltoside-1000, Fe-sucrose and Fe-carboxymaltose rather than indirectly using TSI as a proxy for IVIP-Fe. This matters particularly for Fe-carboxymaltose and Fe-sucrose where the separation between IVIP-Fe and TSI trajectories is particularly apparent (Figure 3BC); thus their $t_{1/2}$ is twice longer with the TSI than the IVIP-Fe method (Table 2). This study shows that, for Fe-carboxymaltose and Fe-sucrose, the assumption that IVIP-Fe=TSI is incorrect, especially for lower doses. We also confirmed relative differences in the IVIP half-lives (Fe-isomaltoside-1000>Fe-carboxymaltose>Fe-sucrose) although the absolute values differed from those published previously[5], most likely due to the lower doses used.
Plasma hepcidin increments after IVIP injection have been described[18,54,55]. Here we show hepcidin peak following the TSAT peak by 20-24h with all IVIPs (Figure 4C,E). This likely reflects the negative feedback between transferrin-$Fe_2$ and hepcidin expression. In hepatocytes TfR1-TfR2-HFE-BMPR interaction positively regulates BMPR signalling to hepcidin transcription[56,57]. This peak-to-peak lag between TSAT and hepcidin is shorter for Fe-sucrose (18-22 hours). One explanation is that

additional positive signalling to hepcidin expression occurs earlier with Fe-sucrose due to higher peak NTBI concentrations. If hepatocyte iron is increased, e.g. rapidly via the NTBI route, this may be sensed by the BMP6 pathway that up-regulates hepcidin expression, and supplements the transferrin-$Fe_2$-dependent TfR2 signalling.

### Two mechanisms of NTBI generation following IVIP administration

We relied on three parameters established to address this subject, namely the differences between IVIPs in the peak time and the magnitude of the rise and fall of NTBI levels relative to the peak time, magnitude and the rate of the rise and fall of s-Ferritin, including the mutual temporal relationships between them.

We propose two mechanisms for the generation of the kinetic profiles of NTBI, Figure 4D,F. The Fe-sucrose-generated NTBI profile features two distinct kinetic components: a rapid onset and an early peak at 4h followed by decay and a secondary peak/shoulder at 16h disappearing at 36h (individual profiles are bi- or tri-modal, but the peak times and magnitudes vary across patients possibly due to the effect of protein corona, not shown). The first peak represents predominantly the rapid release into plasma of weakly-bound iron directly from circulating complexes, because the said 4h peak occurs within the first plasma half-life of Fe-sucrose (henceforth *Pathway 1*). This can occur even when transferrin is not fully saturated and is dependent on rate of release of iron from the formulation, the iron-ligand speciation, and the kinetic binding equilibrium of transferrin[38,43,58]. In contrast, because the second peak/shoulder occurs after 4 half-lives, at which time over 90% of Fe-sucrose has been taken up by macrophages, that 16h NTBI peak predominantly represents indirect, ferroportin-mediated iron efflux from macrophages that fully saturates transferrin (henceforth *Pathway 2*), Figure 6.

With Fe-isomaltoside-1000, given its long plasma half-life, the small NTBI peak at 8h thus represents direct iron release from circulating IVIP, while any indirect release after the first half-life is evidently at much slower macrophage-mediated release rate at which transferrin does not become saturated and consequently NTBI is virtually absent.

Fe-carboxymaltose initially follows the Fe-isomaltoside-1000 NTBI profile corresponding to the direct generation of NTBI, but displays a starkly different behaviour reflecting the indirect macrophage iron release with a late NTBI peak at 24h, at which time ~4 plasma half-lives have already elapsed. This difference between Fe-isomaltoside-1000 and Fe-carboxymaltose may partially be accounted for by differences in plasma half-lives, i.e. by the amount of IVIP having been hitherto taken up by macrophages (>90% of Fe-carboxymaltose and <60% of Fe-isomaltoside-1000).

As for the macrophage-mediated uptake process, chromatography of the IVIPs shows the average size of IVIPs decreasing with time. This effect is more marked for Fe-carboxymaltose and Fe-sucrose than for Fe-isomaltoside-1000 (shift in peak elution time, Figure 2D, Supplement Figure S4). This is best interpreted by macrophages preferentially removing the larger IVIP species and so the smaller species are likely to persist longer in plasma.

The macrophage processing efficiency is higher for Fe-carboxymaltose because, according to the s-Ferritin AUC differences (Figure 5B), 75% more iron per 200mg dose is extracted from Fe-carboxymaltose than Fe-isomaltoside-1000. Plausibly, some unprocessed Fe-isomaltoside-1000 complexes remain in macrophages and are non-bioavailable (at least within 2 weeks, as here). This could be resolved if ferritin were measured sequentially until it reached baseline to enable total s-Ferritin AUC

comparison between IVIPs. This approach would confirm that the complete s-Ferritin AUC represents the fraction of bioavailable iron at a given dose processed by macrophages, which is not reduced by the fraction that escapes via NTBI route (*Pathway 1*) to parenchymal cells. When NTBI is absent or relatively low as in the case of Fe-isomaltoside-1000, the difference in complete s-Ferritin AUC between e.g. Fe-carboxymaltose and Fe-isomaltoside-1000 could mean that a sizeable proportion of the Fe-isomaltoside-1000 iron remains unprocessed in macrophages. Whether that is due to inherent structural properties of some IVIPs or to dysregulation of iron metabolism e.g. high hepcidin in haemodialysis[18,59,60] or both, remains to be determined. Nevertheless, the relative magnitude of iron shunted away from IVIP via the NTBI plasma compartment to parenchymal cells (hepatocytes) is small (estimated approximately 1000-times smaller) as compared with the iron flux directed to the erythron from IVIP via the TBI compartment, Supplement Figure S6.

The proposed NTBI generation *Pathways 1 and 2* can be corroborated by comparing NTBI profiles with the rate of s-Ferritin increase (Figure 4D vs. Figure 4F). As s-Ferritin reports macrophage iron content[61,62], at 16 hours after Fe-sucrose injection it is already half-maximal (s-Ferritin=~80µg/L), at which time we observe a second NTBI peak/shoulder of ~0.7µM (indicating high rate iron egress exceeding the transferrin iron binding capacity). The fact that for Fe-sucrose at 4h the ~1.3µM NTBI peak (and ~0.8µM at 2h) does not correspond to any s-Ferritin increase indicates that the NTBI cannot have arisen from the macrophage compartment, which thus confirms the existence of two separate NTBI generation pathways.

IVIPs typically become a source of iron for metabolic pathways after they have been processed by macrophages[16]. Macrophage uptake rate can be inferred from plasma half-life of IVIPs, whereas endolysosomal IVIP degradation rate following macrophage uptake can be inferred from the rate of s-Ferritin increase. S-Ferritin increases in plasma as a marker of the iron stored in macrophage cellular ferritin, which undergoes turnover via the transient labile iron pool that regulates ferritin mRNA translation via IRP-IRE system[61]. Importantly, the faster the IVIP disappears from plasma, the faster s-Ferritin increases (compare IVIP-Fe $t_{1/2}$ and the exponential association constant of s-Ferritin increase, Figure 5D), suggesting that the different physicochemical characteristics of the IVIP that influence half-life[6,7] are likely to be the fundamental reason for this relationship and hence for the differential iron bioavailability. Thus, Fe-isomaltoside-1000 is a relatively inert polymer taking longer to be removed by macrophages and longer to release bioavailable iron (60h longer than Fe-sucrose and 24h longer than Fe-carboxymaltose), Figure 5A.

Significantly, the s-Ferritin decay rate is similar across IVIPs (Figure 5A) suggesting a common mechanism of iron egress (macrophage ferroportin), once released from IVIP within endolysosomes. This iron egress (hence its bioavailability) can be inferred from the fall of macrophage iron stores as reported by falling s-Ferritin.

Similarly, albeit less clearly, IVIP half-life correlates with exposure to NTBI (NTBI AUC), but without associating with either the exposure to TSAT or to hepcidin, Supplement Figure S2A-C. This is consistent with NTBI generation resulting from IVIP rapidly loading the macrophage compartment and iron rapidly egressing (*Pathway 2*) against a hitherto relatively low hepcidin level (thus open ferroportin) where that hepcidin level later increases in response to increased plasma Transferrin-

$Fe_2$. The rapidity of NTBI appearance with Fe-sucrose vs. Fe-carboxymaltose or Fe-isomaltoside-1000 strongly suggests that ambient iron is immediately made available in plasma for exchange with transferrin until its saturation (*Pathway 1*) before further iron is released via macrophage ferroportin. Rapid NTBI release *in vitro* from buffered Fe-sucrose was abrogated following 1h incubation with normal serum, confirming the released NTBI as apotransferrin-exchangeable (Supplement Figure S5). Thus, Fe-sucrose is more labile than the other IVIPs, consistent with our clinical observations, Figure 4D. This *in vitro* NTBI behavior may result from rapid reconstitution of alkaline Fe-sucrose solution (pH 10-11) in plasma pH (7.4) with speciation changes enabling iron donation to the CP851 chelator (or, by extension, an endogenous chelator *in vivo* e.g. plasma citrate) more rapidly than with Fe-carboxymaltose or Fe-isomaltoside-1000. Furthermore, the protein corona could make a contribution to the stability of the iron core and macrophage processing of that is unique to each IVIP formulation.

Late onset of NTBI appearance with Fe-carboxymaltose strongly suggests that it becomes available to macrophage ferroportin much later, and that the initial rapid release from the formulation directly is negligible (Supplement Figure S5). The crystalline (i.e. more stable) akaganeite-like form of Fe-carboxymaltose iron may be digested differently within endolysosomes than the less well defined structure of Fe-sucrose iron[5]. Although Fe-isomaltoside-1000 and Fe-carboxymaltose both possess akaganeite structures, the core size in Fe-isomaltoside-1000 is smaller[5]. Thus, differential stability between these two preparations may be explained by different carbohydrate shells or different core sizes of the crystalline iron (hence more significant differences in surface area)[6].

The results of this study should be considered in the context of some limitations. Firstly, the IVIPs were all administered at 200 mg doses of elemental iron, which was required to accurately evaluate the complex pharmacokinetic profiles of each formulation. Thus, following the successful model developed in this work, doses that are clinically administered should be studied in the future. It is possible that larger doses may increase NTBI generation by pathway 2 or that AUC of s-Ferritin greatly increases if there is a transition from linear to zero-order elimination. Secondly this study did not directly compare different NTBI assays and evaluate their association with the pharmacokinetic and pharmacodynamic profiles of the iron-carbohydrate nano-medicines, however, this is the subject of ongoing work from our group.

In conclusion, IVIP pharmacokinetics and pharmacodynamics support a two-pathway model of NTBI release. Although all IVIPs are iron sources, the rate and extent of iron bioavailability differs, following over a 2 week-period the sequence Fe-carboxymaltose>Fe-sucrose>Fe-isomaltoside-1000. This strengthens the notion of IVIPs as pro-drugs that should not be considered interchangeable. The potential clinical consequences of NTBI on long-term iron bioavailability, efficacy and safety remain unknown and require further studies.

## Acknowledgements

The authors would like to thank Andrew Cakebread who operated the HPLC-ICPMS at KCL and Simon Cheesman who provided the intravenous iron preparations. Vifor Pharma provided blood samples and additional study data. JP would like to acknowledge UCL Biomedical Research Centre for Cardiometabolic Programme Support.

## References


1. Garbowski MW, Ma Y, Fucharoen S, Srichairatanakool S, Hider R, Porter JB. Clinical and methodological factors affecting non-transferrin-bound iron values using a novel fluorescent bead assay. Transl Res. 2016;177:19-30.e5.
2. de Swart L, Hendriks JCM, van der Vorm LN, et al. Second international round robin for the quantification of serum non-transferrin-bound iron and labile plasma iron in patients with iron-overload disorders. Haematologica. 2016;101(1):38-45.
3. Evans RW, Rafique R, Zarea A, et al. Nature of non-transferrin-bound iron: Studies on iron citrate complexes and thalassemic sera. J Biol Inorg Chem. 2008;13(1):57-74.
4. Porter JB, Garbowski M. The pathophysiology of transfusional iron overload. Hematol Oncol Clin North Am. 2014;28(4):683-701.
5. Neiser S, Rentsch D, Dippon U, et al. Physico-chemical properties of the new generation IV iron preparations ferumoxytol, iron isomaltoside 1000 and ferric carboxymaltose. BioMetals. 2015;28(4):615-635.
6. Geisser P. Why Different Iron(III)-oxyhydroxide Complexes have Different PK/PD Characteristics and Specific Reactivities. J Pharm Nanotechnol. 2016;4(1):14-18.
7. Bhandari S, Pereira DIA, Chappell HF, Drakesmith H. Intravenous irons: From basic science to clinical practice. Pharmaceuticals. 2018;11(3):1-20.
8. Koskenkorva-Frank TS, Weiss G, Koppenol WH, Burckhardt S. The complex interplay of iron metabolism, reactive oxygen species, and reactive nitrogen species: Insights into the potential of various iron therapies to induce oxidative and nitrosative stress. Free Radic Biol Med. 2013;65:1174-1194.
9. Neiser S, Koskenkorva TS, Schwarz K, Wilhelm M, Burckhardt S. Assessment of dextran antigenicity of intravenous iron preparations with enzyme-linked immunosorbent assay (ELISA). Int J Mol Sci. 2016;17(7):1185.
10. Jahn MR, Andreasen HB, Fütterer S, et al. A comparative study of the physicochemical properties of iron isomaltoside 1000 (Monofer®), a new intravenous iron preparation and its clinical implications. Eur J Pharm Biopharm. 2011;78(3):480-491.
11. Geisser P, Burckhardt S. The pharmacokinetics and pharmacodynamics of iron preparations. Pharmaceutics. 2011;3(1):12-33.
12. Rangel ÉB, Espósito BP, Carneiro FD, et al. Labile plasma iron generation after intravenous iron is time-dependent and transitory in patients undergoing chronic hemodialysis. Ther Apher Dial. 2010;14(2):186-192.
13. Espósito BP, Breuer W, Slotki I, Cabantchik ZI. Labile iron in parenteral iron formulations and its potential for generating plasma nontransferrin-bound iron in dialysis patients. Eur J Clin Invest. 2002;32(s1):42-49.
14. Ma Y, Podinovskaia M, Evans PJ, et al. A novel method for non-transferrin-bound iron quantification by chelatable fluorescent beads based on flow cytometry. Biochem J. 2014;463(3):351-362.
15. Danielson BG. Structure, chemistry, and pharmacokinetics of intravenous iron agents. J Am Soc Nephrol. 2004;15(SUPPL. 2):93-98.
16. Geisser P, Baer M, Schaub E. Structure/histotoxicity relationship of parenteral iron preparations. Arzneimittelforschung. 1992;42(12):1439-1452.
17. Pai AB, Conner T, McQuade CR, Olp J, Hicks P. Non-transferrin bound iron, cytokine activation and intracellular reactive oxygen species generation in hemodialysis patients receiving intravenous iron dextran or iron sucrose.

BioMetals. 2011;24(4):603-613.
18. Kitsati N, Liakos D, Ermeidi E, et al. Rapid elevation of transferrin saturation and serum hepcidin concentration in hemodialysis patients after intravenous iron infusion. Haematologica. 2015;100(3):e80-83.
19. Danielson BG, Salmonson T, Derendorf H, Geisser P. Pharmacokinetics of iron(III)-hydroxide sucrose complex after a single intravenous dose in healthy volunteers. Arzneimittelforschung. 1996;46(6):615-621.
20. Food and Drug Administration (FDA). Draft Guidance on Iron Sucrose. 2012;2012-2013.
21. Bansal SS, Halket JM, Fusova J, et al. Quantification of hepcidin using matrix-assisted laser desorption/ ionization time-of-flight mass spectrometry. Rapid Commun Mass Spectrom. 2009;23(11):1531-1542.
22. Nguyen VH, Lee B-J. Protein corona: a new approach for nanomedicine design. Int J Nanomedicine. 2017;12:3137-3151.
23. Brissot P, Ropert M, Le Lan C, Loréal O. Non-transferrin bound iron: A key role in iron overload and iron toxicity. Biochim Biophys Acta. 2012;1820(3):403-410.
24. Loreal O, Gosriwatana I, Guyader D, Porter J, Brissot P, Hider RC. Determination of non-transferrin-bound iron in genetic hemochromatosis using a new HPLC-based method. J Hepatol. 2000;32(5):727-733.
25. al-Refaie FN, Wickens DG, Wonke B, Kontoghiorghes GJ, Hoffbrand AV. Serum non-transferrin-bound iron in beta-thalassaemia major patients treated with desferrioxamine and L1. Br J Haematol. 1992;82(2):431-436.
26. Inati A, Musallam KM, Wood JC, Sheikh-Taha M, Daou L, Taher AT. Absence of cardiac siderosis by MRI T2* despite transfusion burden, hepatic and serum iron overload in Lebanese patients with sickle cell disease. Eur J Haematol. 2009;83(6):565-571.
27. Porter JB, Walter PB, Neumayr LD, et al. Mechanisms of plasma non-transferrin bound iron generation: insights from comparing transfused diamond blackfan anaemia with sickle cell and thalassaemia patients. Br J Haematol. 2014;167(5):692-696.
28. Porter JB, Lin KH, Beris P, et al. Response of iron overload to deferasirox in rare transfusion-dependent anaemias: Equivalent effects on serum ferritin and labile plasma iron for haemolytic or production anaemias. Eur J Haematol. 2011;87(4):338-348.
29. Santini V, Girelli D, Sanna A, et al. Hepcidin levels and their determinants in different types of myelodysplastic syndromes. PLoS One. 2011;6(8):e23109.
30. Cortelezzi a, Cattaneo C, Cristiani S, et al. Non-transferrin-bound iron in myelodysplastic syndromes: a marker of ineffective erythropoiesis? Hematol J. 2000;1(3):153-158.
31. Bradley SJ, Gosriwitana I, Srichairatanakool S, Hider RC, Porter JB. Non-transferrin-bound iron induced by myeloablative chemotherapy. Br J Haematol. 1997;99(2):337-343.
32. Sahlstedt L, Ebeling F, von Bonsdorff L, Parkkinen J, Ruutu T. Non-transferrin-bound iron during allogeneic stem cell transplantation. Br J Haematol. 2001;113(3):836-838.
33. Garbowski MW, Evans P, Vlachodimitropoulou E, Hider R, Porter JB. Residual erythropoiesis protects against myocardial hemosiderosis in transfusion-dependent thalassemia by lowering labile plasma iron via transient generation of apotransferrin. Haematologica. 2017;102(10):1640-1649.

34. Garbowski MW, Ma Y, Fucharoen S, Srichairatanakool S, Hider R, Porter JB. Clinical and methodological factors affecting non-transferrin-bound iron values using a novel fluorescent bead assay. Trans Res. 2016;177:19-30.e5.
35. Porter JB, Cappellini MD, Kattamis A, et al. Iron overload across the spectrum of non-transfusion-dependent thalassaemias: role of erythropoiesis, splenectomy and transfusions. Br J Haematol. 2016;176(2):288-299.
36. Schmann K, Kroll S, Romero-Abal ME, et al. Impact of oral iron challenges on circulating non-transferrin-bound iron in healthy guatemalan males. Ann Nutr Metab. 2012;60(2):98-107.
37. Schümann K, Solomons NW, Orozco M, Romero-Abal ME, Weiss G. Differences in circulating non-transferrin-bound iron after oral administration of ferrous sulfate, sodium iron EDTA, or iron polymaltose in women with marginal iron stores. Food Nutr Bull. 2013;34(2):185-193.
38. Dresow B, Petersen D, Fischer R, Nielsen P. Non-transferrin-bound iron in plasma following administration of oral iron drugs. Biometals. 2008;21(3):273-276.
39. Hutchinson C, Al-Ashgar W, Liu DY, Hider RC, Powell JJ, Geissler CA. Oral ferrous sulphate leads to a marked increase in pro-oxidant nontransferrin-bound iron. Eur J Clin Invest. 2004;34(11):782-784.
40. Esposito BP, Breuer W, Sirankapracha P, Pootrakul P, Hershko C, Cabantchik ZI. Labile plasma iron in iron overload: Redox activity and susceptibility to chelation. Blood. 2003;102(7):2670-2677.
41. Erichsen K, Ulvik RJ, Grimstad T, Berstad A, Berge RK, Hausken T. Effects of ferrous sulphate and non-ionic iron-polymaltose complex on markers of oxidative tissue damage in patients with inflammatory bowel disease. Aliment Pharmacol Ther. 2005;22(9):831-838.
42. Khalid S, Shaikh F, Moeen S. Decreased activity of glutathione peroxidase with oral ferrous iron administration: A cause of oxidative stress. Pak J Pharm Sci. 2018;31(2):405-409.
43. Pai AB, Boyd AV, McQuade CR, Harford A, Norenberg JP, Zager PG. Comparison of oxidative stress markers after intravenous administration of iron dextran, sodium ferric gluconate, and iron sucrose in patients undergoing hemodialysis. Pharmacotherapy. 2007;27(3):343-350.
44. Kuo KL, Hung SC, Lee TS, Tarng DC. Iron sucrose accelerates early atherogenesis by increasing superoxide production and upregulating adhesion molecules in CKD. J Am Soc Nephrol. 2014;25(11):2596-2606.
45. Kshirsagar AV, Freburger JK, Ellis AR, Wang L, Winkelmayer WC, Brookhart MA. Intravenous iron supplementation practices and short-term risk of cardiovascular events in hemodialysis patients. PLoS One. 2013;8(11):e78930.
46. Macdougall IC, White C, Anker SD, et al. Intravenous iron in patients undergoing maintenance hemodialysis. N Engl J Med. 2019;380(5):447-458.
47. Brookhart MA, Freburger JK, Ellis AR, Wang L, Winkelmayer WC, Kshirsagar AV. Infection risk with bolus versus maintenance iron supplementation in hemodialysis patients. J Am Soc Nephrol. 2013;24(7):1151-1158.
48. Macdougall IC, Bhandari S, White C, et al. Intravenous Iron Dosing and Infection Risk in Patients on Hemodialysis: A Prespecified Secondary Analysis of the PIVOTAL Trial. J Am Soc Nephrol. 2020;31(5):1118-1127.
49. Schümann K, Solomons NW, Romero-Abal ME, Orozco M, Weiss G, Marx J. Oral administration of ferrous sulfate, but not of iron polymaltose or sodium

iron ethylenediaminetetraacetic acid (NaFeEDTA), results in a substantial increase of non-transferrin-bound iron in healthy iron-adequate men. Food Nutr Bull. 2012;33(2):128-136.
50. Scheiber-Mojdehkar B. Non-Transferrin-Bound Iron in the Serum of Hemodialysis Patients Who Receive Ferric Saccharate: No Correlation to Peroxide Generation. J Am Soc Nephrol. 2004;15(6):1648-1655.
51. Van Veldhuisen DJ, Ponikowski P, Van Der Meer P, et al. Effect of Ferric Carboxymaltose on Exercise Capacity in Patients with Chronic Heart Failure and Iron Deficiency. Circulation. 2017;136(15):1374-1383.
52. Lewis GD, Malhotra R, Hernandez AF, et al. Effect of oral iron repletion on exercise capacity in patients with heart failure with reduced ejection fraction and iron deficiency the IRONOUT HF randomized clinical trial. JAMA. 2017;317(19):1958-1966.
53. Ambrosy AP, Lewis GD, Malhotra R, et al. Identifying responders to oral iron supplementation in heart failure with a reduced ejection fraction: A post-hoc analysis of the IRONOUT-HF trial. J Cardiovasc Med. 2019;20(4):223-225.
54. Gaillard CA, Bock AH, Carrera F, et al. Hepcidin Response to Iron Therapy in Patients with Non-Dialysis Dependent CKD: An Analysis of the FIND-CKD Trial. PLoS One. 2016;11(6):e0157063.
55. Zehra A, Saleh Abdullah SM, Saboor M, Moinuddin. Effect of Intravenous Iron Supplementation on Hepcidin Levels in Iron Deficient Pregnant Females in Second and Third Trimester. Indian J Hematol Blood Transfus. 2017;33(3):396-401.
56. Lin L, Valore E V, Nemeth E, Goodnough JB, Gabayan V, Ganz T. Iron transferrin regulates hepcidin synthesis in primary hepatocyte culture through hemojuvelin and BMP2/4. Blood. 2007;110(6):2182-2189.
57. Ganz T. Hepcidin and iron regulation, 10 years later. Blood. 2011;117(17):4425-4433.
58. Lee DH, Ding YL, Jacobs DR, et al. Common presence of non-transferrin-bound iron among patients with type 2 diabetes. Diabetes Care. 2006;29(5):1090-1095.
59. Wish JB. Assessing iron status: beyond serum ferritin and transferrin saturation. Clin J Am Soc Nephrol. 2006;1 Suppl 1:S4-S8.
60. Wish JB, Aronoff GR, Bacon BR, et al. Positive Iron Balance in Chronic Kidney Disease: How Much is Too Much and How to Tell? Am J Nephrol. 2018;47(2):72-83.
61. Rouault TA, Stout CD, Kaptain S, Harford JB, Klausner RD. Structural relationship between an iron-regulated RNA-binding protein (IRE-BP) and aconitase: Functional implications. Cell. 1991;64(5):881-883.
62. Torti FM, Torti S V. Regulation of ferritin genes and protein. Blood. 2002;99(10):3505-3516.

# Tables

## Table 1

Table 1. Baseline parameters.

| Blood test | FCM, n=8 | IIM, n=8 | IS, n=8 | Placebo, n=4 | All, n=28 |
|---|---|---|---|---|---|
| **Females** | 7 | 7 | 7 | 4 | 25 |
| **C-Reactive Protein [mg/L]** | 1.47 ± 2.18 | 0.85 ± 0.84 | 0.96 ± 0.65 | 0.34 ± 0.16 | 0.98 ± 1.29 |
| **Serum Ferritin [µg/L]** | 14.24 ± 8.8 | 10.94 ± 4.77 | 15.05 ± 10.39 | 8.26 ± 4.33 | 12.67 ± 7.89 |
| **Hemoglobin [g/L]** | 126.5 ± 5.42 | 125.5 ± 9.42 | 128.37 ± 11.23 | 123.25 ± 4.64 | 126.28 ± 8.28 |
| **Hepcidin [ng/mL]** | 1.07 ± 1.2 | 1.36 ± 2.17 | 3.27 ± 2.52 | 0.67 ± 0.76 | 1.72 ± 2.16 |
| **Iron [µmol/L]** | 10.34 ± 5.11 | 13.04 ± 5.89 | 9.46 ± 4.75 | 12.69 ± 5.68 | 11.2 ± 5.26 |
| **NTBI [µmol/L]** | 0.0 ± 0.0 | 0.0 ± 0.0 | 0.0 ± 0.0 | 0.0 ± 0.0 | 0.0 ± 0.0 |
| **Reticulocytes [10^9/L]** | 61.8 ± 10.88 | 56.81 ± 13.99 | 53.75 ± 18.51 | 60.97 ± 29.43 | 57.95 ± 16.67 |
| **Soluble Transferrin Receptor [mg/L]** | 1.49 ± 0.41 | 1.3 ± 0.13 | 1.26 ± 0.45 | 1.47 ± 0.25 | 1.36 ± 0.34 |
| **Transferrin [g/L]** | 3.0 ± 0.4 | 2.9 ± 0.28 | 2.84 ± 0.18 | 3.1 ± 0.2 | 2.94 ± 0.29 |
| **Transferrin Saturation [%]** | 13.81 ± 7.05 | 18.07 ± 8.41 | 13.55 ± 7.57 | 16.65 ± 8.28 | 15.36 ± 7.6 |
| **UIBC [µmol/L]** | 56.68 ± 9.3 | 50.95 ± 8.29 | 53.97 ± 8.01 | 58.35 ± 10.28 | 54.51 ± 8.72 |

FCM, ferric carboxymaltose; IIM, iron isomaltoside 1000; IS, iron sucrose; NTBI, non-transferrin bound iron; UIBC, unsaturated iron binding capacity. Values given as mean±SD

## Table 2

Table 2. Selected pharmacokinetic parameters of IVIPs

| Biomarker | PK parameter | ferric carboxymaltose, n=8 | Iron isomaltoside 1000, n=8 | Iron sucrose, n=8 |
|---|---|---|---|---|
| **IVIP-Fe** | $c_{max}$, mean±SD [mmol/L] | 1.16±0.09 | 1.29±0.1 | 0.85±0.17 |
| | $t_{max}$, mean (min-max) [h] | 0.34 (0.33-0.7) | 0.67 (0.33-6) | 0.35 (0.33-0.37) |
| | t½, mean±SD [h] | 6.82±1.93 | 20.3±2.27 | 3.43±1.55 |
| | $AUC_{0\text{-}inf}$ [h*mmol/L] | 12.39±1.2 | 36.76±4.9 | 2.59±0.5 |
| **TSI** | $c_{max}$, mean±SD [mmol/L] | 1.18±0.1 | 1.3±0.1 | 0.89±0.21 |
| | $t_{max}$, mean (min-max) [h] | 0.33 (0.18-0.7) | 0.68 (0.33-6) | 0.34 (0.18-0.37) |
| | t½, mean±SD [h] | 11.14±3.42 | 19.21±2.97 | 7.5±1.76 |
| | $AUC_{0\text{-}inf}$ [h*mmol/L] | 14.8±1.22 | 38.5±4.13 | 4±0.53 |
| **TBI** | $c_{max}$, mean±SD [mmol/L] | 49.13±7.19 | 38.34±10.8 | 51.27±4.68 |
| | $t_{max}$, mean (min-max) [h] | 24 (4-24) | 8.05 (6-24) | 5 (4-24) |
| | t½, mean±SD [h] | 11.45±4.88 | 15.35±4.44 | 6.82±1.38 |
| | $AUC_{0\text{-}inf}$ [h*mmol/L] | 2.09±0.42 | 1.72±0.49 | 1.37±0.28 |

TSI, total serum iron; TBI transferrin-bound iron; $c_{max}$, maximal plasma concentration;
$t_{max}$, time of maximal plasma concentration; t½ plasma half-life,
$AUC_{0\text{-}inf}$, area-under-curve from zero to infinity;

## Figure legends

### Figure legend 1

Figure 1. Bead-NTBI assay. (A) Side-scatter-area vs. forward-scatter-area plot, gate P1 identifies a population of CP-851 beads; (B) side-scatter-area vs. side-scatter-height plot, gate P3 excludes doublets; (C) histogram of FITC-area from combination of P1 and P3 gates, shown with an example statistics (right), median of the distribution represents the bead fluorescence; (D) All 28 standard curves (each in triplicate) plotted together with mean and SD shown (n=84), 4-parameter logistic curve fitted $r^2$=0.97; (E) example standard curve with mean and SD shown (triplicates), logM units were transformed by exponentiation and multiplied by $1.0x10^6$ to obtain results in µmol/L; (F) overlay histograms of FITC-area, as in C above, for buffer (0µM Fe-NTA standard), control serum, a patient sample in duplicate extrapolated at 1.02µM NTBI and 10µM Fe-NTA standard, see inset; (G) overlay of FITC-area histograms showing a standard curve example. Limit of Blank ($95^{th}$ percentile of 8 replicates, LoB) was 0.51nM, Limit of Detection (LoB-$1.654SD_{(low\ standard)}$, LoD) 14.6nM, Limit of Quantitation (LoQ) 30 nM, intra-assay and inter-assay precision CVs were 1.28% and 4.34% respectively (28 consecutively run assays over 82 days, with triplicate controls).

### Figure legend 2

Figure 2. Chromatography of the IVIPs using HPLC-ICPMS at KCL. (A) An example serum sample HPLC-ICPMS run with integration of chromatograms within the Chromera software. (B) The subtraction chromatograms of IVIPs in serum samples (ex vivo), baseline subtracted from the 4h time-point. Variable abundance is a function of the given IVIP half-life at 4h; transferrin peak (at 13.2 min) indicates the iron exchange from IVIP to apotransferrin. The precision of subtraction is validated by the overlay of the internal standard (not shown) converging on 15µM FO (subtraction of 5µM from 20µM). (C) The subtraction chromatograms of IVIPs (30µM) incubated in vitro with 20% serum for 1h with control chromatograms subtracted. Distinct chromatograms for Fe-isomaltoside-1000, Fe-sucrose and Fe-carboxymaltose identified. Small iron signal at 13.2 min is ferrotransferrin testifying to exchange of labile iron between polymers and apotransferrin. (D) Comparison of in-vitro (thick) and ex-vivo (thin) IVIP chromatograms from B and C using two y-axes for peak size adjustment. At 4h post-infusion patient samples show distinct shift of the peak elution time, which indicates that principal IVIP species changes with time i.e. that larger species are preferentially removed from plasma. Fe-carboxymaltose shows greatest shift of peak time.

### Figure legend 3

Figure 3. Aggregate profiles of key iron metabolism parameters. IVIP is infused at time 0h (red arrow), with time<0h indicating baseline values, see legend for graph explanation: NTBI (black) is plotted on the right y-axis, all other variables – on the log axis (left y-axis); note hepcidin concentration is multiplied by 10 to enable plotting on the log axis. (A) Fe-isomaltoside-1000, n=8; (B) Fe-sucrose, n=8; (C) Fe-carboxymaltose, n=8; (D) Placebo, n=4.

### Figure legend 4

Figure 4. Aggregate data of IVIP-Fe, total serum iron, transferrin saturation, NTBI, hepcidin and ferritin for all patients. Data shown in aggregate for treatment groups:

placebo (blue), Fe-carboxymaltose (red), Fe-isomaltoside-1000 (black), Fe-sucrose (green). (A) IVIP-Fe plasma concentrations (log scale in the inset), estimated from pre-Transferrin chromatographic peak AUCs; (B) total serum iron (log scale in the inset) (C) transferrin saturation (TSAT); (D) NTBI, x-axis limited to 48h as no appearance of NTBI post after 48 hours was observed; (E) plasma hepcidin (10*ng/mL); (F) serum ferritin during the initial 48 hours for direct comparison with NTBI in D.

## Figure legend 5

Figure 5. Serum ferritin behaviour on study. (A) Cumulative serum ferritin profiles for treatment groups, fitted using global fitting with a custom function (plateau followed by mono-exponential association followed by mono-exponential decay), SEM, global fit R square 0.84; (B) box-and-whisker plots of ferritin AUCs (baseline-312h); (C) box-and-whisker plots of ferritin mono-exponential association rate constant $K_{assoc}$; (D) Relationships of the rate of increase in serum ferritin to the plasma half-life of the IVIP.

## Figure legend 6

Figure 6. Schematic model of IVIP-dependent generation of NTBI from two compartments. Before IVIPs are eventually taken up by macrophages, small proportion of circulating IVIPs may directly release loosely bound iron as NTBI or release iron at sufficiently high rate to generate NTBI despite apotransferrin (ApoTf) presence in hypoferremic state (Pathway I: Direct release from IVIP). Following macrophage uptake, ferroportin (Fpn)-dependent release of NTBI (Pathway II, Macrophage-mediated release) is the default NTBI route.

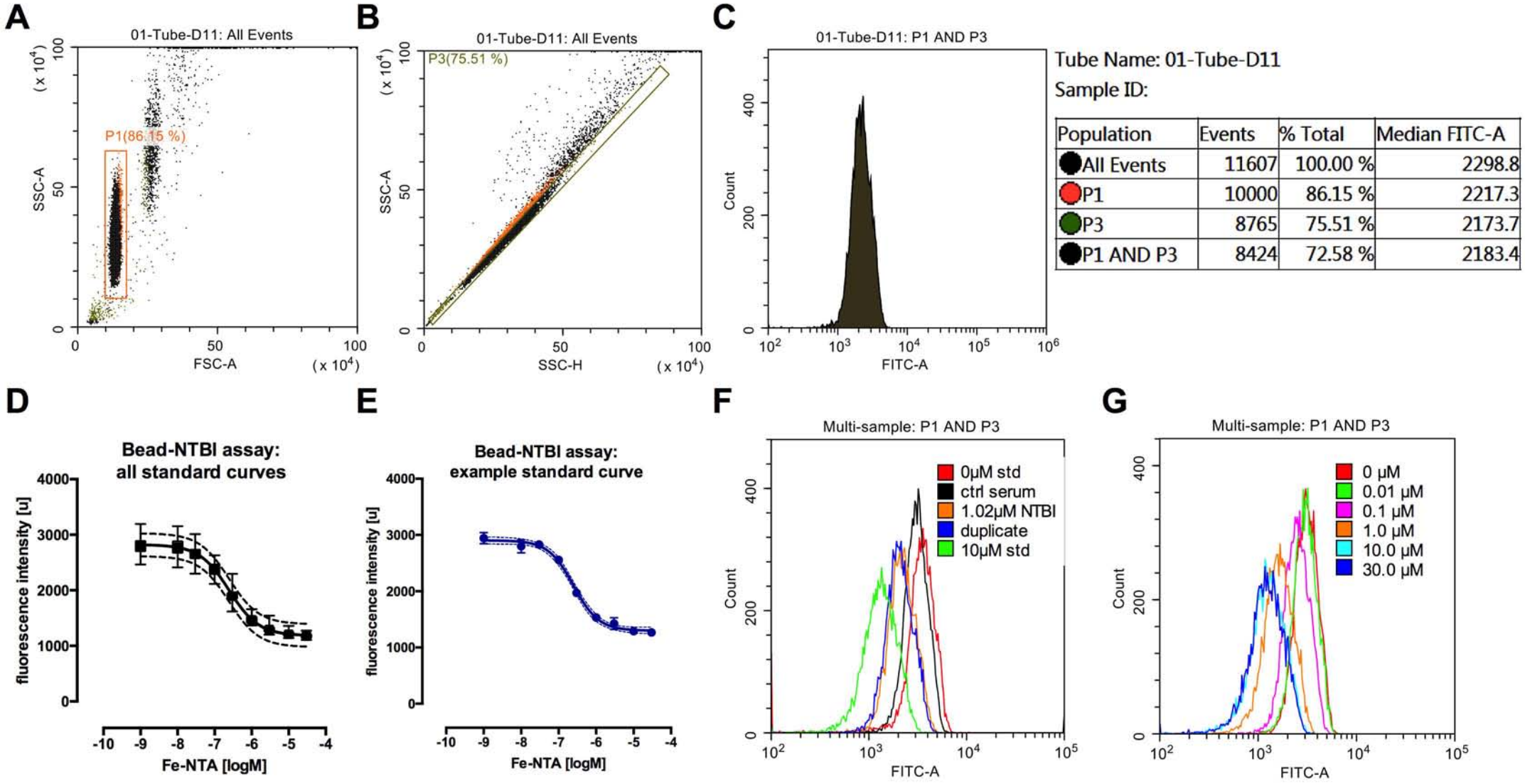
A
01-Tube-D11: All Events
P1(86.15 %)
SSC-A
FSC-A
B
01-Tube-D11: All Events
P3(75.51 %)
SSC-A
SSC-H
C
01-Tube-D11: P1 AND P3
Count
FITC-A
Tube Name: 01-Tube-D11
Sample ID:
Population | Events | % Total | Median FITC-A
All Events | 11607 | 100.00 % | 2298.8
P1 | 10000 | 86.15 % | 2217.3
P3 | 8765 | 75.51 % | 2173.7
P1 AND P3 | 8424 | 72.58 % | 2183.4
D
Bead-NTBI assay:
all standard curves
fluorescence intensity [u]
Fe-NTA [logM]
E
Bead-NTBI assay:
example standard curve
fluorescence intensity [u]
Fe-NTA [logM]
F
Multi-sample: P1 AND P3
0μM std
ctrl serum
1.02μM NTBI
duplicate
10μM std
Count
FITC-A
G
Multi-sample: P1 AND P3
0 μM
0.01 μM
0.1 μM
1.0 μM
10.0 μM
30.0 μM
Count
FITC-A

**FIGURE 1**

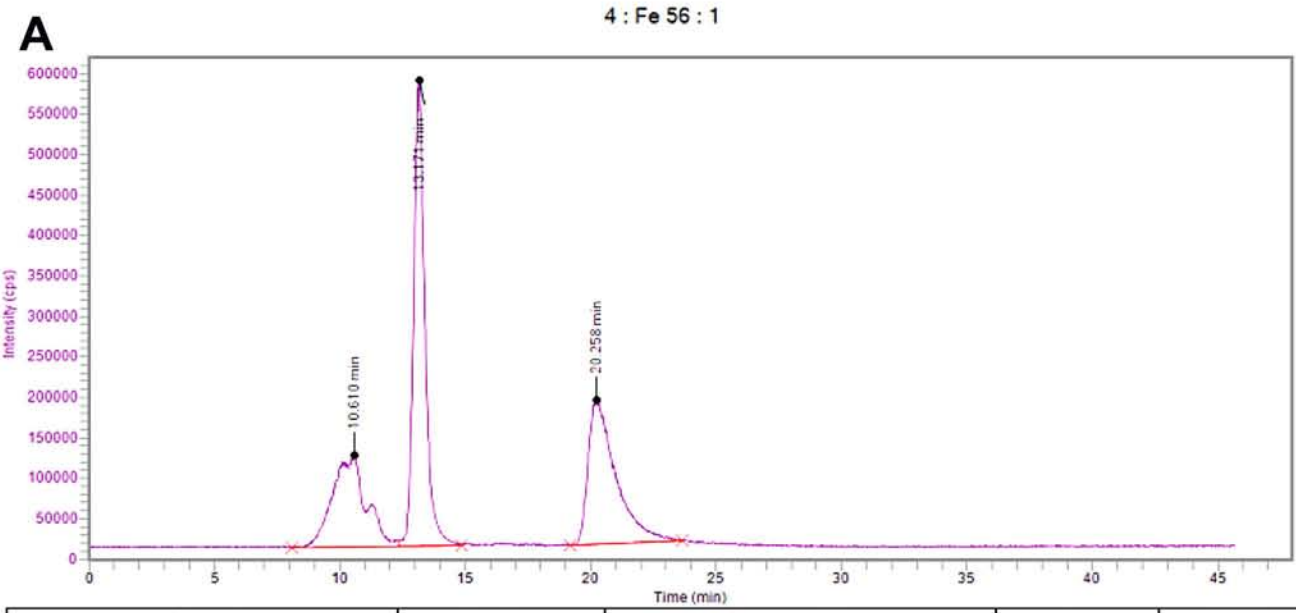


| Channel | Ret. Time | Component Name | Area | Height |
|---|---|---|---|---|
| Fe 56 | 10.60991109 | pre-Transferrin peaks | 10519662.98 | 113063.9122 |
| Fe 56 | 13.17109842 | Transferrin peak | 17854454.22 | 575310.628 |
| Fe 56 | 20.25766477 | Ferrioxamine internal standard | 13824470.87 | 177936.5324 |

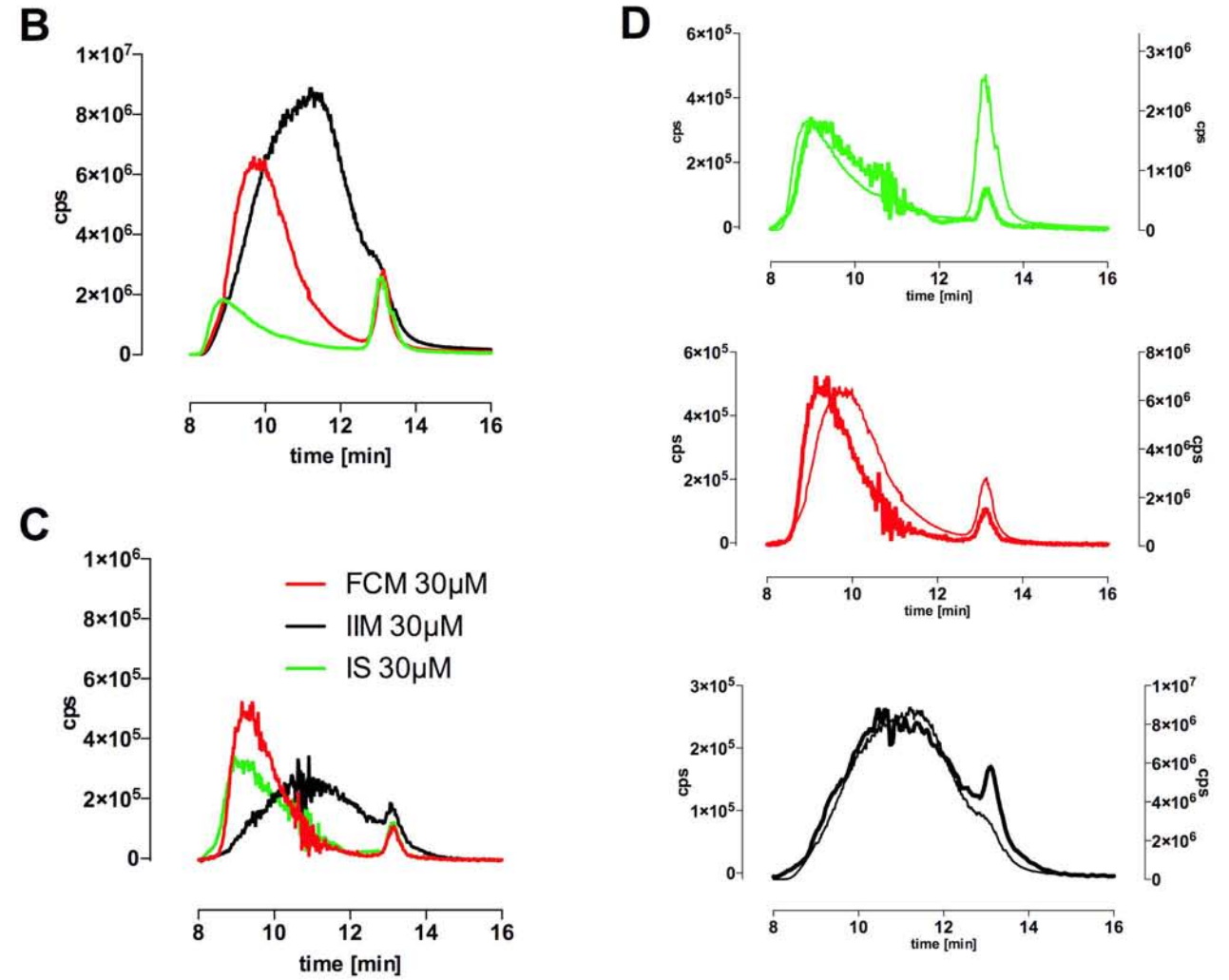


**FIGURE 2**

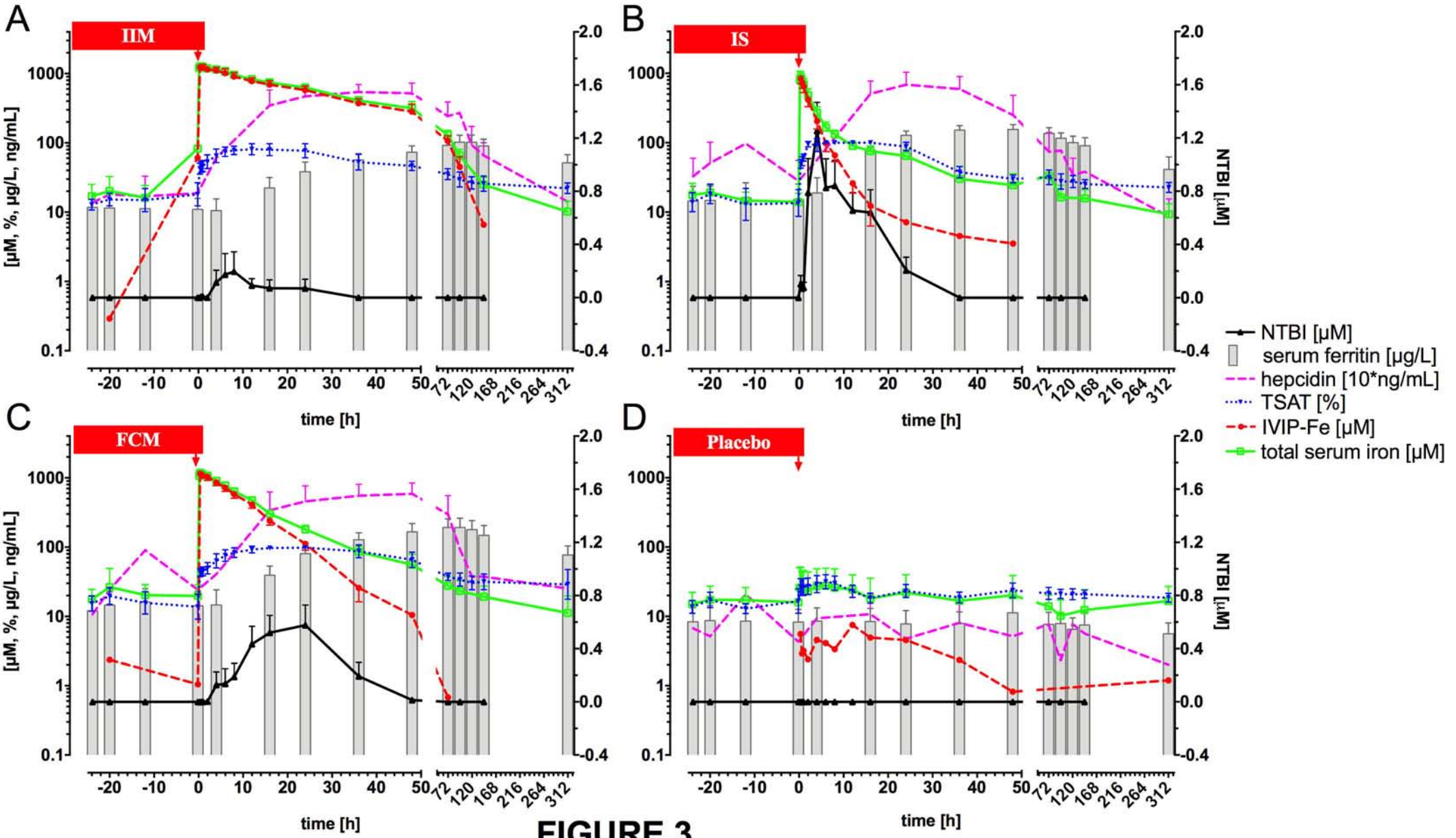
A
IIM
B
IS
C
FCM
D
Placebo
[µM, %, µg/L, ng/mL]
NTBI [µM]
time [h]
-20 -10 0 10 20 30 40 50 72 120 168 216 264 312
0.1 1 10 100 1000
-0.4 0.0 0.4 0.8 1.2 1.6 2.0
NTBI [µM]
serum ferritin [µg/L]
hepcidin [10*ng/mL]
TSAT [%]
IVIP-Fe [µM]
total serum iron [µM]

**FIGURE 3**

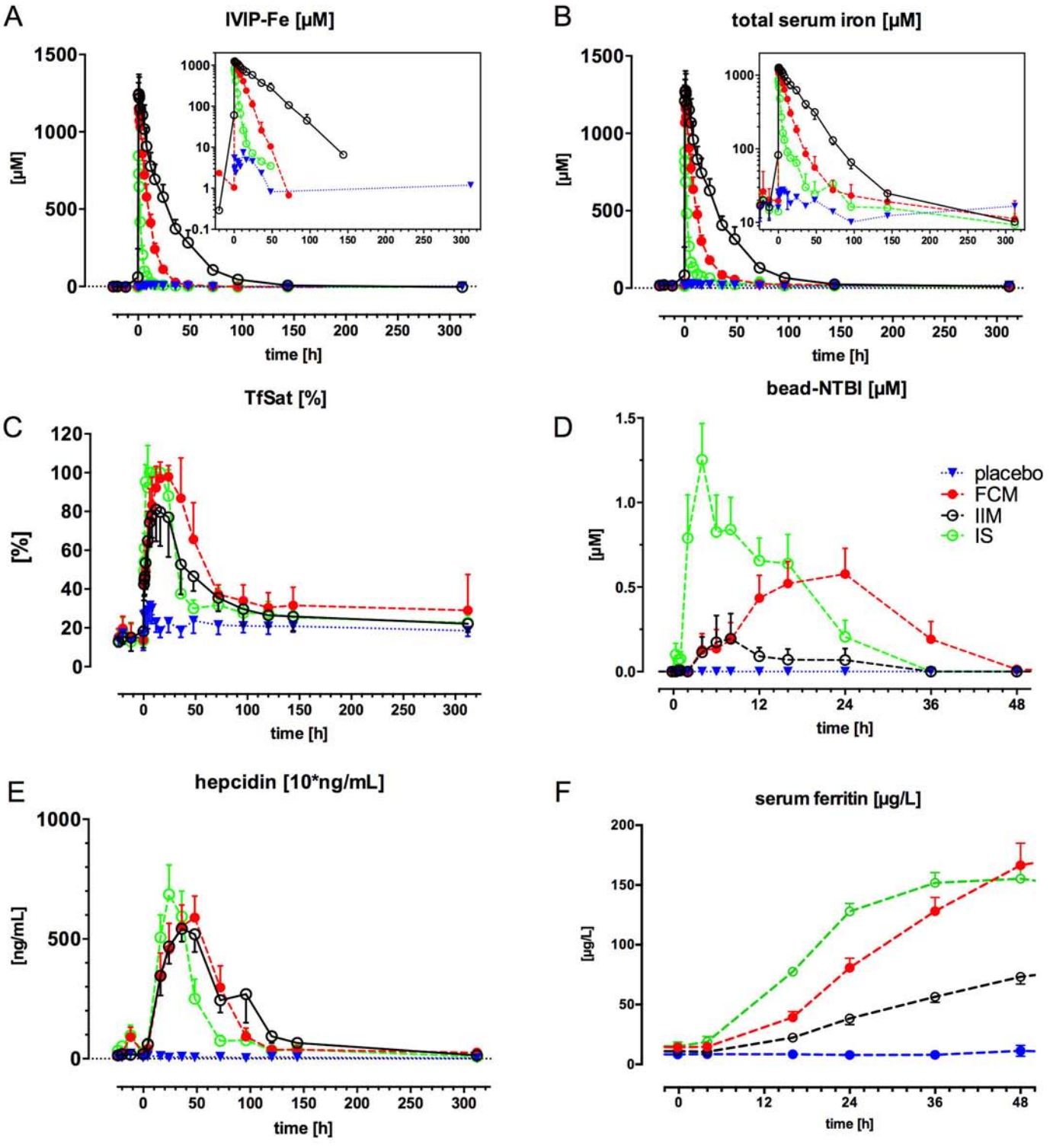
A
IVIP-Fe [µM]
[µM]
time [h]
B
total serum iron [µM]
[µM]
time [h]
C
TfSat [%]
[%]
time [h]
D
bead-NTBI [µM]
[µM]
time [h]
placebo
FCM
IIM
IS
E
hepcidin [10*ng/mL]
[ng/mL]
time [h]
F
serum ferritin [µg/L]
[µg/L]
time [h]

FIGURE 4

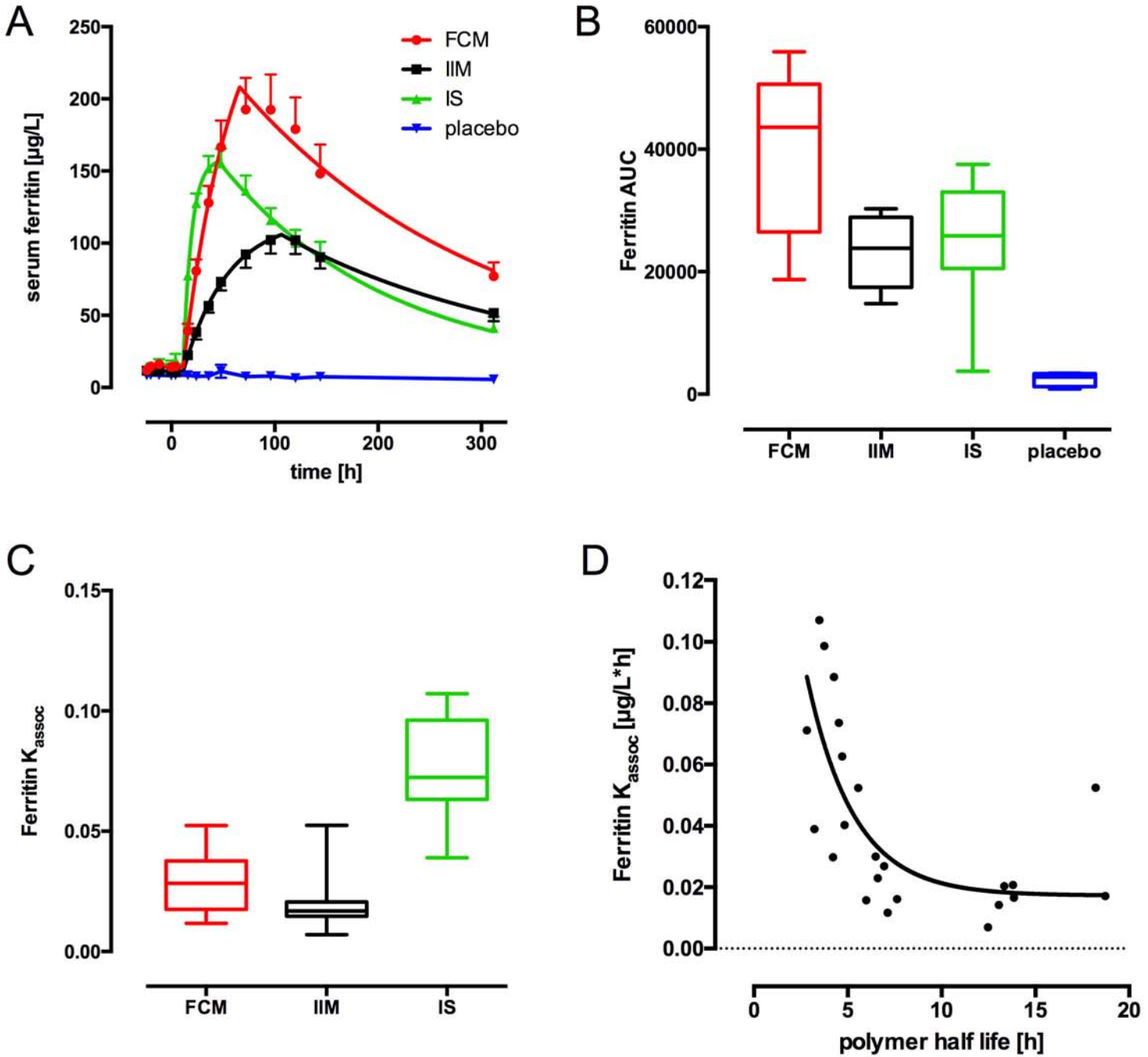
A
250
200
150
100
50
0
serum ferritin [µg/L]
FCM
IIM
IS
placebo
0
100
200
300
time [h]
B
60000
40000
20000
0
Ferritin AUC
FCM
IIM
IS
placebo
C
0.15
0.10
0.05
0.00
Ferritin K assoc
FCM
IIM
IS
D
0.12
0.10
0.08
0.06
0.04
0.02
0.00
Ferritin K assoc [µg/L*h]
0
5
10
15
20
polymer half life [h]

**FIGURE 5**

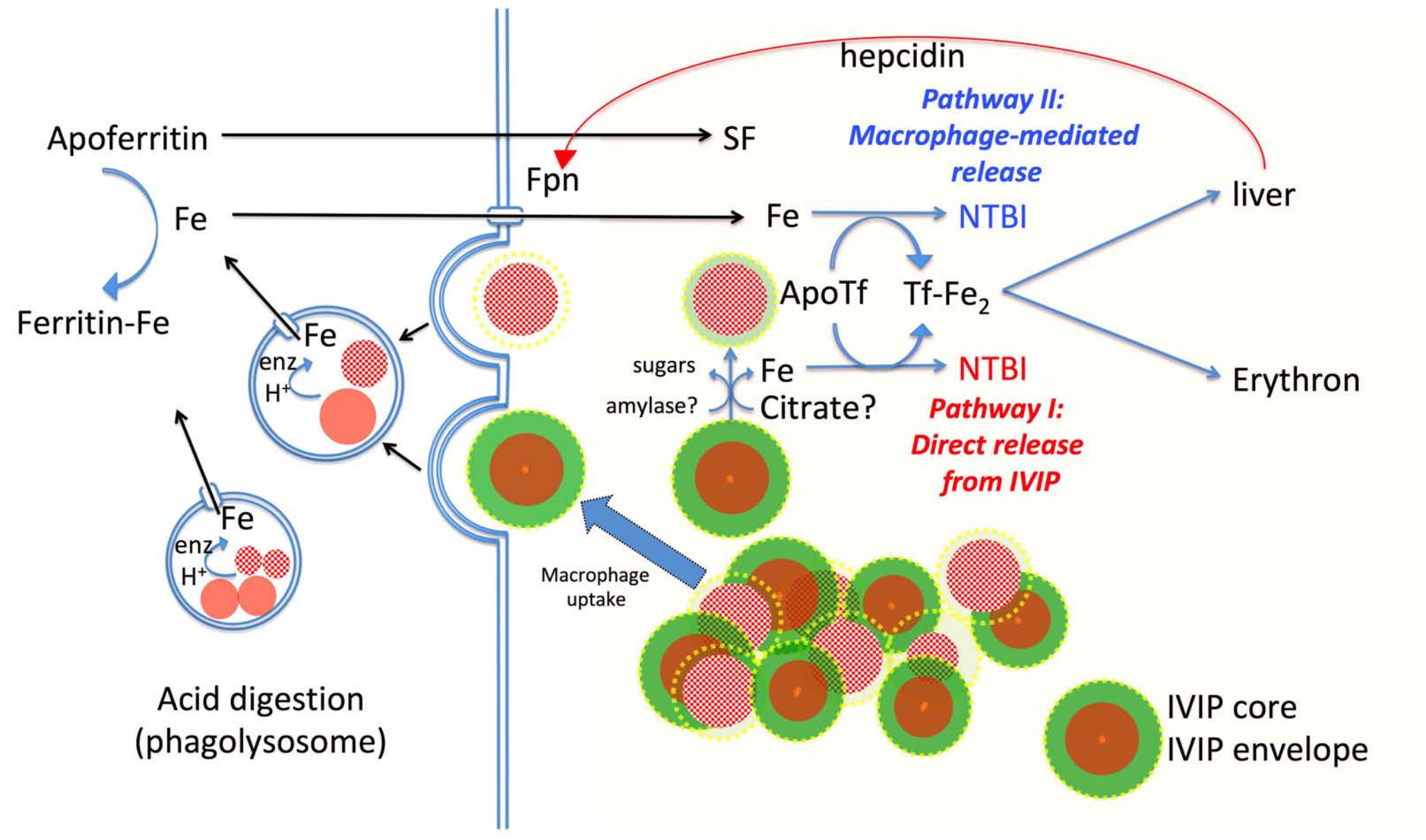
hepcidin
Pathway II:
Macrophage-mediated
release
Apoferritin
SF
Fpn
Fe
Fe
NTBI
liver
Ferritin-Fe
ApoTf
Tf-Fe2
Fe
enz
H+
sugars
amylase?
Fe
Citrate?
NTBI
Erythron
Pathway I:
Direct release
from IVIP
Fe
enz
H+
Macrophage
uptake
Acid digestion
(phagolysosome)
IVIP core
IVIP envelope

**Intravenous iron preparations transiently generate non-transferrin-bound iron from two proposed pathways**

Maciej W. Garbowski, MD PhD; Sukhvinder Bansal PhD; John B. Porter, MA MD FRCP FRCPath; Claudio Mori MD; Susanna Burckhardt PhD; Robert C. Hider PhD

# Supplement

## Supplementary Methods: Bead NTBI assay

We used the previously published bead-NTBI method[1,2] with some modifications. The hexadentate CP851 chelator is covalently bound to a fluorescein moiety on the beads. Upon binding of iron to CP851 chelator on the beads, fluorescence is quenched proportionally to the amount of iron bound. This in turn is proportional to iron concentration in solution.

### Standards preparation

All buffer solutions were made up from analytical grade chemicals and AnalaR NORMAPUR HPLC-grade water (VWR) and treated with Chelex® 100 sodium form (Sigma) to remove contaminating iron.

Ferric nitrilotriacetate (Fe-NTA, Sigma) standards were prepared from stock solutions and filtered using a 0.22µm syringe filter (Nylon P/N:FIL-S-PP-022-13-100 13mm x 0.22µm, Racing Green, Chromatography). 45µL of 20mM NTA stock solution was transferred to a 15mL Falcon tube to which 20µL of 18mM ferric nitrate atomic absorption iron standard solution (Fluka) was added; the tube was vortexed and 835µL of AnalaR water was added to a total of 900µL, whereupon the solution was left for 1h to equilibrate at room temperature. This generated 400µM Fe-NTA at 1:2.5 ratio. Adding a further 11.1mL of AnalaR water to this solution made up 12mL of the 30µM Fe-NTA standard, which was subsequently kept frozen at -20ºC as 500µL aliquots. The aliquots were used on the day of the assay to generate the serial dilution solutions for the standard curve (30, 10, 3, 1, 0.3, 0.1, 0.03, 0.01, 0µM).

### Sample preparation

Serum samples were thawed at room temperature (bench-top) then vortexed and filtered using a 0.22µm syringe filter (as above) with the filtrates (250µL) centrifuged at 14,000 rpm for 10 minutes.

### Assay procedure

The assay buffer 150mM NaCl 50mM 3-(N-morpholino)propanesulfonic acid (MOPS, VWR) buffer, pH 7.4, was chelexed overnight. 20µL of serum supernatant (diluted 5-fold in buffer solution, i.e. 10µL in 40µL buffer), was transferred to the labeled wells in an acid-washed (100mM HCL, Fisher) dry 96-well plate in duplicate. Freshly prepared Fe-NTA (1:2.5) standards, 20µL, were added in triplicate to the designated wells (without dilution). 5-Fold diluted control normal serum, 20µL, was added in triplicate to the designated wells. Next, the CP851 beads, suspended in freshly prepared buffer, were added. Stock solution of the beads was 4.8 x $10^7$/mL (synthesized at Prof Yongmin Ma laboratory, School of Pharmaceutical Science, Zhejiang Chinese Medical University, Hangzhou, China). This was diluted 16-fold to 3.0 x $10^6$/mL in buffer). Typically 18mL of the bead suspension in buffer was prepared and 180µL of the suspension aliquoted to each well. The plate was then transferred to a plate shaker at a low stirring level for 20h-incubation at 37ºC.

### Flowcytometry procedure

We used the Beckman Coulter CytoFLEX flow-cytometer with CytExpert software, KCL. Beads were identified on a side-scatter-area vs. forward-scatter-area plot as a uniform population of events (gate P1, see Figure 1A). Bead doublets were identified and excluded on a side-scatter-area vs. side-scatter-height plot (gate P3 excluding doublets). On a histogram plot for the FITC fluorescence channel, a median of the distribution (gated as P1 AND P3) was taken as the value representing the bead fluorescence. Exclusion gating (P4) corrects for auto-fluorescence (not shown).

### Data analysis

Data was gathered at 10,000 events per gate P1 on a fast (60µL/min) setting. Median fluorescence was extracted for samples, controls and standards and analyzed using a standard curve modeled in GraphPad Prism 6.0 software with a 4-parameter logistic function, see Figure 1DE, with iron concentration in logM units. The interpolated unknowns were transformed by exponentiation and multiplied by $1.0x10^6$ to obtain results in µmol/L, and corrected for the dilution factor.

### Quality control

Instrument validation was performed before each use. This involved system start-up procedure, Quality Control using CytoFLEX daily QC Fluorospheres (Beckman Coulter B53230) for laser calibration, and daily clean with a Beckman Coulter cleaning solution and distilled water.
Limit of Blank ($95^{th}$ percentile of 8 replicates, LoB) 0.51nM, Limit of Detection ($LoB-1.654SD_{(low\ standard)}$, LoD) 14.6nM, Limit of Quantitation (LoQ) 30 nM, intra-assay and inter-assay precision CVs were 1.28% and 4.34% respectively (28 consecutively run assays over 82 days, with triplicate controls).

## Supplementary Methods: Plasma Hepcidin measurement at KCL

Hepcidin standard was purchased from Peptides International and a working solution was prepared in methanol:water:formic acid (49:49:2) at a concentration of 100 µg/mL. The net peptide content was determined by amino acid analysis. This solution was aliquoted into a total recovery vials and then freeze-dried, stoppered and stored at -80ºC. The internal standard, $[^{13}C_9,^{15}N_1]Phe^{4,9}$-hepcidin(H-IS) was synthesized in-house and prepared similarly to hepcidin. All standards and QC samples were prepared in rabbit plasma (Sigma P4550). The samples and standards were allowed to thaw at room temperature and 200µL aliquot of each sample, standard or QC sample was transferred into a low binding multi-well plate, and 50µL of a 1.0µg/mL H-IS solution prepared in rabbit plasma added. Samples were mixed followed by the addition of 300µL of 4% phosphoric acid. Samples were mixed and then centrifuged at 5000 rcf for 10 minutes. Solid phase extraction wells were first conditioned with 200µL of methanol followed by equilibration with 200µL water. The supernatant was loaded onto the extraction plate. Samples were washed with 1% formic acid and hepcidin was eluted with 25µL of 40:50:10 of acetonitrile: 0.1% formic acid: trifluoroethanol (elution solvent).
Ten microliters of the eluent were chromatographed using an ACQUITY UPLC on an Acquity BEH 130 column, 1.7 µm, and 2.1 x 50 mm. The gradient elution solvents were 0.1% formic acid in water: acetonitrile: trifluoroethanol (90:5:5) (mobile phase A) and 0.1% formic acid in acetonitrile: water: trifluoroethanol (90:5:5) (mobile phase B), the sample was eluted on a linear gradient from 20% B to 60% B in 2

minutes at a flow rate of 200 µl/min. For hepcidin and H-IS, collision induced dissociation products of multiple charged precursors were detected in the positive ion selected reaction monitoring mode using a Waters Xevo TQS mass spectrometer. The electrospray voltage, source temperature, desolvation temperature and desolvation gas flow rate were 3.0 kV, 150 °C, 500 °C and 1000 L/hr, respectively. Selected reaction monitoring (SRM) transitions used for quantitation were for hepcidin 698.160 > 644.129 and the internal standard 702.777 > 648.741 both with a cone voltage of 20 and a collision energy of 16 eV. MassLynx version 4.1 was used for data acquisition. All peak area integration, regression analysis and sample quantitation was performed using TargetLynx. Specifically, peak area ratios of hepcidin and the internal standard were determined and calibration curves generated using a 1/concentration weighted linear regression model. All QC sample concentrations were then calculated from their peak area ratios against the calibration curves. Re-validated assay data is published previously (supplementary).[3]

## Supplementary Methods: Inductively-Coupled Plasma Mass-Spectrometry (ICPMS) serum analyses (KCL)

### Sample preparation

Samples were thawed at room temperature (bench-top) then vortexed and filtered using a 0.22µm syringe filter (Nylon P/N:FIL-S-PP-022-13-100 13mm x 0.22µm, Racing Green, Chromatography). Filtrates (250µL) were centrifuged at 14,000 rpm for 10 minutes and 90µL of the serum supernatant was transferred to an HPLC glass vial with a plastic insert, 10µL of 180µM ferrioxamine standard (from stock solution kept at 4 deg C throughout the study) was added, and the vials were capped. Final concentration of ferrioxamine in each sample was 18µM, which itself diluted the serum by 10%. Internal standard mean elution time across 16 runs over 158 days was 20.76±1.33min (range 18.34-22.52min) giving a between-run (inter-day) CV of 6.4%. The within-run (intra-day) CV was 0.74±0.43% (range 0.11-1.59%) and was below the 5% critical QC threshold for admissibility of run results.

### Instrument

Perkin Elmer Flexar HPLC (LC Autosampler, LC Pump, Solvent Manager, UV/VIS Detector, Column Oven) coupled to a Perkin Elmer NexION 350 D Inductively-Coupled Plasma Mass Spectrometer (ICP-MS) was used with Syngistix and Chromera operating software (KCL). All instruments were operated strictly according to manufacturers' instructions. The LC UV/Vis detector was set at 254nm. Sample manager was set to a single injection volume of 10µL. A size exclusion column Bio SEC-5, 300Å, 7.8x300mm (Agilent Technologies) equilibrated from storage, was used with a guard column (Agilent Bio SEC-5, guard, 5µm, 500Å, 7.8x50mm) and cleaned every 32 injection-runs, as per manufacturer's instructions.
Isocratic flow was set at 0.75mL/min at room temperature using a mobile phase (50mM ammonium acetate pH 7.4 based on AnalaR NORMAPUR HPLC grade water) with each run lasting 45 minutes, without washing between sample runs but with wash after the last sample-run.
All media solutions were vacuum-filtered using an assembled manifold (Vacuum filtration manifold phenomenex, Millipore) with a 0.22µm Millipore filter and de-gassed in a sonicator for 30 minutes at room temperature before HPLC use.
The following ICP-MS conditions were used: dynamic reaction cell (DRC) mode: nebuliser flow 0.95-1.00 L/min, auxilliary gas flow 1.2 L/min, plasma gas flow

18L/min, RF power 1600 W, ammonia gas flow 0.6mL/min, RPq 0.8, analyte Fe56 (55.9349) dwell time 200ms.
The results were reviewed and integrated within Chromera software (Figure 2A), data analysis was performed on GraphPad Prism Ver 6.0 and custom MS Excel templates.

### IVIP iron in plasma

IVIP iron (IVIP-Fe) co-eluted with the endogenous pre-Tf protein-associated iron, which is a cluster of typically 3 peaks that run before transferrin (13.17min), Figure 2A. IVIP-Fe was integrated and quantitated against the internal standard (FO). Where IVIP-Fe co-eluted with the transferrin peak itself, the transferrin peak was tangentially skimmed and not included in the integration. In order to correct for the endogenous pre-Tf protein-associated iron, the baseline value of the latter (-10min from the IVIP injection) was subtracted from every subsequent chromatographic profile thus providing the estimation of IVIP-Fe. This subtraction represents changes in plasma IVIP-Fe, where the subtracted baseline value (of pre-Tf protein-associated iron) is typically <0.1% of the peak value. Alternatively, IVIP-Fe was also calculated by subtracting TBI from TSI. Plasma half-life of the IVIP-Fe was derived from fitting mono-exponential models of the decay of the IVIP-Fe levels and from non-compartmental analysis (alongside other PK parameters).

## Supplementary Results: Serum ferritin iron content

The pre-Tf protein-associated iron at baseline elutes typically with 3 peaks between 10 and 11.5 minutes (Figure 2A, blue trace in Figure S1A, Figure S1B, Figure S1C). As evident from the placebo profile in Figure S1D, these peaks are changing dynamically over the 312h of follow up. In principle, they represent 3 separate protein species that each carry iron. Potential candidates at that molecular weight range include haptoglobin-Hb complex, and ferritin. However, the baseline of the pre-Tf protein-associated iron may be compared to its end-of-study level, and assuming all else being equal (e.g. haptoglobin-Hb complex), the difference in pre-Tf iron in that comparison (EOS-baseline) should represent the change in ferritin iron content on study. At baseline (-10 min), no IVIPs are present and at 312h sufficient number of half-lives have elapsed for the IVIPs to be completely removed. On that assumption, the change in serum ferritin iron content from 312 hours back to baseline was negative on average but highly variable and the change was not statistically significant (Figure S2D).

## Supplementary Results: Erythropoietic response

All patients were non-anaemic at baseline, and there was no difference in Hb between treatment groups at baseline (Table 1). As a result of frequent blood sampling throughout the study (total volume 424mL), patient Hb levels sustained a downward trend; this needs to be considered in the context of low dose of IVIP being administered. The degree of Hb reduction is significant between baseline and EOS (ANOVA time effect $p<0.0001$, mean reduction 7.2±1.1 g/L at 312h). Nevertheless, there was no difference between treatment groups in the degree to which Hb level was reduced at the end of study due to the cumulative phlebotomies on study (Figure S3 left). Essentially, what was administered as IVIP iron was removed as RBC iron. Reticulocyte percentage count increased with time and across treatment modalities (data not shown). Whether that was as a result of multiple blood sampling, loading with iron, or both, cannot be definitively established in this study. Similar behaviour

was observed for sTfR, however the increases in sTfR were only significant for IS and placebo (Figure S3 right).

## Supplementary Figures

### Figure S1

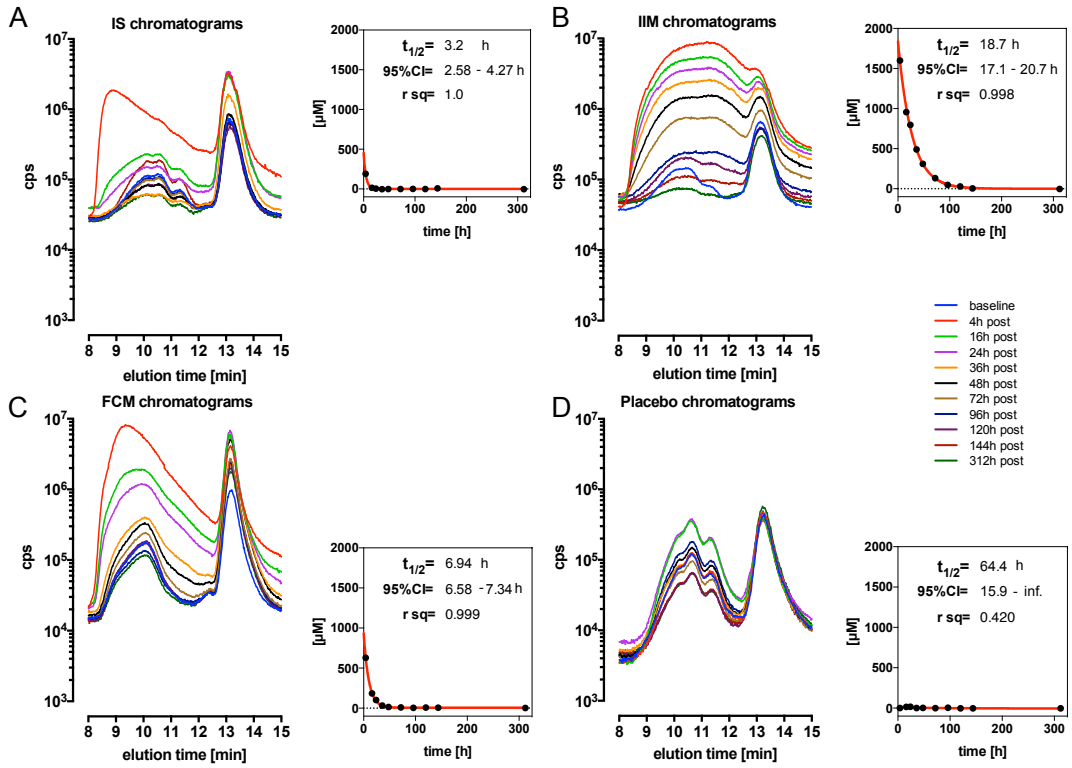


Figure S1. Overlay of chromatograms from all time-points within an example patient from each study arm. Chromatograms, with counts-per-second (cps) on a log scale to enhance resolution, were shown between 8 and 15 min elution time for 11 consecutive samples from baseline to 312h, see legend. Respective insets show mono-exponential decay fits of the post-$C_{max}$ data derived from pre-Tf peak AUCs corrected for baseline AUC, with fitted values of the half-life of the IVIP shown. (A) iron sucrose (IS) chromatograms, (B) iron isomaltoside 1000 (IIM) chromatograms, (C) ferric carboxymaltose (FCM) chromatograms, and (D) Placebo chromatograms.

**Figure S2**

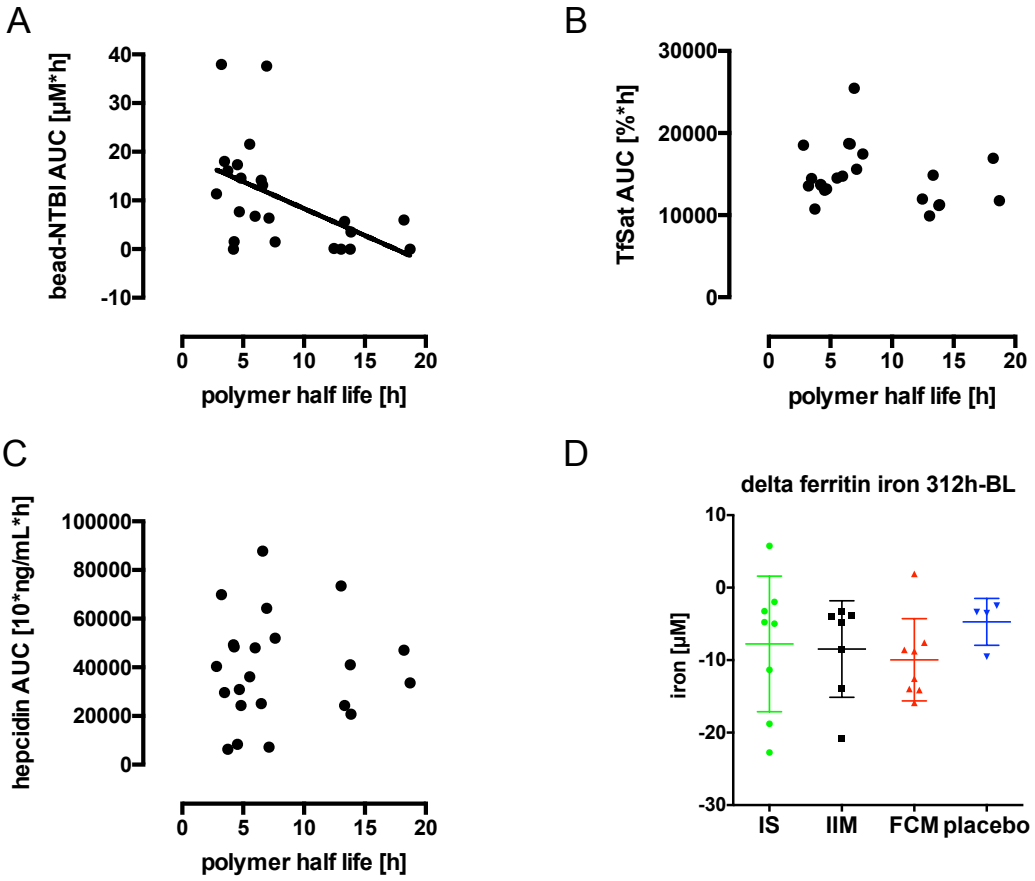


Figure S2. Relationships of plasma half-life of the iron polymers with (A) NTBI AUC, Spearman correlation -0.58, p=0.0041 (B) TSAT AUC, p>0.05 (ns) (C) hepcidin AUC, p>0.05 (ns). (D) Change in serum ferritin iron content on study, estimated from the difference in the pre-Tf peaks (312h minus baseline), shown as replicates with mean±SD for all treatment groups; n=8 for each IVIP, n=4 for placebo.

**Figure S3**

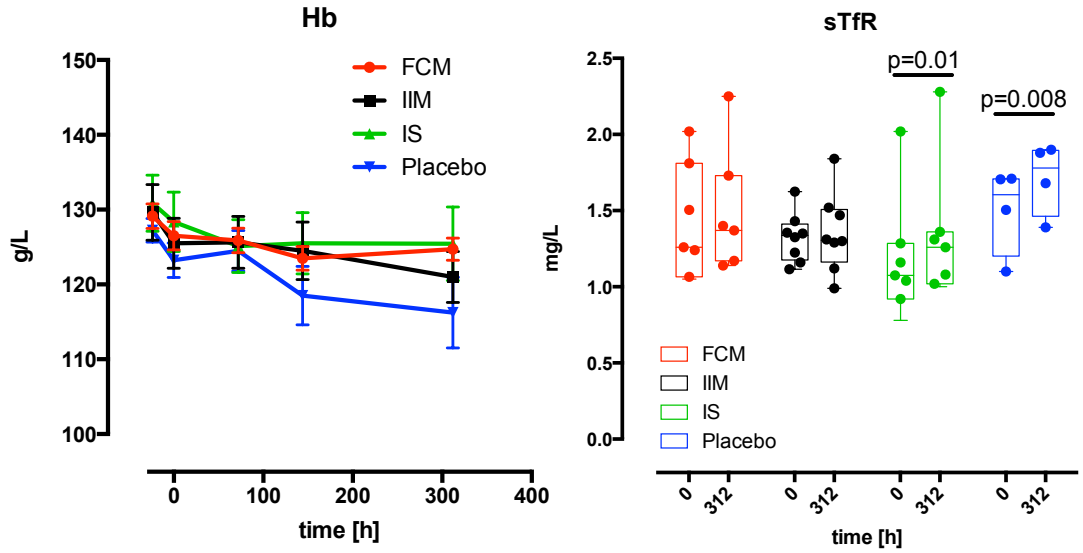


Figure S3. Erythropoietic response on study. Haemoglobin trend on study (left panel); sTfR comparison 0 vs. 312h within treatment groups and placebo, Two-way ANOVA with respect to time and treatment and Holm-Sidak's multiple comparison test p values shown where significant (right panel).

**Figure S4**

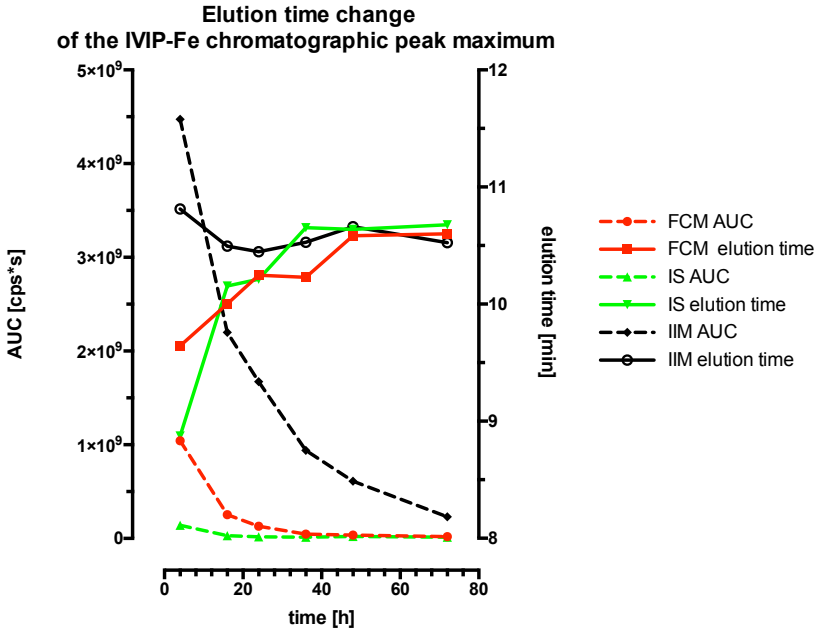


Figure S4. Change in the IVIP-Fe chromatographic peak elution time with respect to time on study. Chromatographic AUC values for each IVIP-Fe peak (left axis) are paired with the respective elution time (right axis) for each peak at the respective time-point and regressed on the study time (4-72h from baseline). Example date shown for IIM, FCM and IS.

**Figure S5**

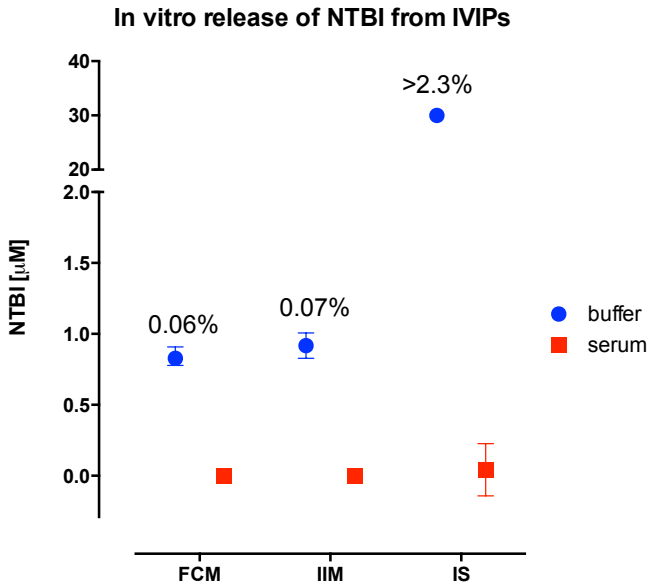


Figure S5. The in vitro NTBI release from IVIPs using the CP851-NTBI assay. 1.3mM IVIP iron was incubated for 1h at room temperature with 150mM NaCl 50mM MOPS pH 7.4 buffer or normal serum before being assayed by the NTBI assay, data shown as median±range, n=3. NTBI as a percentage of total IVIP iron (1.3mM) is shown. Disappearance of NTBI during incubation with serum confirms the NTBI as exchangeable with transferrin. The IS buffer NTBI value of 30µM is at the upper limit of the assay, so should be interpreted as >30µM.

**Figure S6**

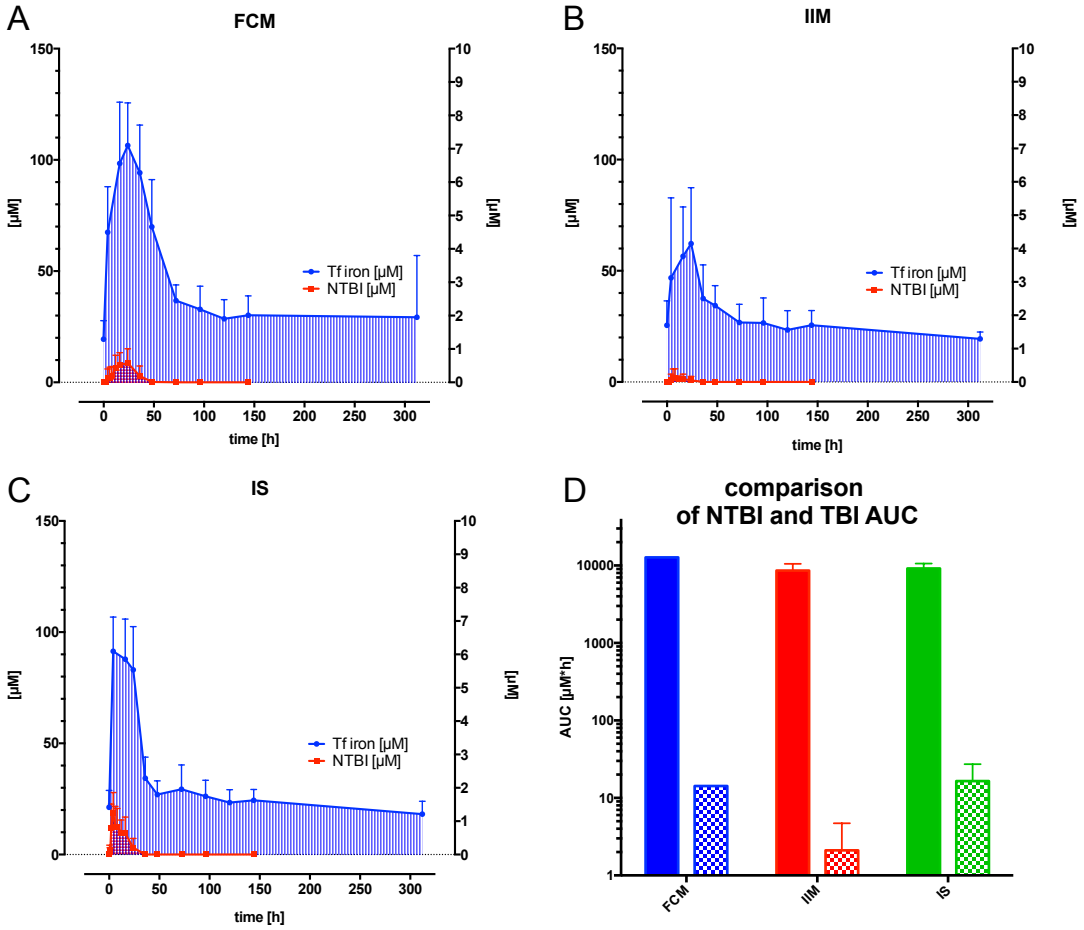


Figure S6. Comparison of TBI and NTBI exposure as AUC between IVIP treatments. TBI AUC is shown on the left axis while NTBI AUC on the right axis is exaggerated 15-fold for visual clarity. (A) FCM, (B) IIM, (C) IS, (D) comparison of TBI and NTBI AUCs in selfsame units (µM*h), shows that NTBI AUC is ≤0.1% of TBI AUC.

## References


1. Garbowski MW, Ma Y, Fucharoen S, et al. Clinical and methodological factors affecting non-transferrin-bound iron values using a novel fluorescent bead assay. *Transl. Res.* 2016;177:19-30.e5.
2. Ma Y, Podinovskaia M, Evans PJ, et al. A novel method for non-transferrin-bound iron quantification by chelatable fluorescent beads based on flow cytometry. *Biochem J.* 2014;463(3):351–362.
3. Pechlaner R, Kiechl S, Mayr M, et al. Correlates of serum hepcidin levels and its association with cardiovascular disease in an elderly general population. *Clin. Chem. Lab. Med.* 2016;54(1):151–161.